

**NUMERICAL MODELING OF WAVE  
OVERTOPPING AND OVERWASH OF DUNE  
FRONTED WITH PILE FENCE**

BY

REBECCA QUAN AND NOBUHISA KOBAYASHI

RESEARCH REPORT NO. CACR-14-09  
NOVEMBER 2014



**CENTER FOR APPLIED COASTAL RESEARCH**

Ocean Engineering Laboratory  
University of Delaware  
Newark, Delaware 19716

## **ACKNOWLEDGMENTS**

This study was supported partly by the U.S. Army Corps of Engineers under Contract No. W911XK-13-P-0065.

## TABLE OF CONTENTS

LIST OF TABLES .....	iv
LIST OF FIGURES .....	v
ABSTRACT .....	ix

### Chapter

1 INTRODUCTION .....	1
2 EXPERIMENT .....	3
3 DATA ANALYSIS .....	7
4 NUMERICAL MODEL .....	14
5 COMPARISON OF MODEL WITH MEASURED DATA .....	18
6 CONCLUSIONS .....	24
REFERENCES .....	26

### Appendix

A PROFILE COMPARISONS .....	28
B FREE SURFACE, VELOCITY, AND WET PROBABILITY COMPARISONS.....	32
C EXTREME FREE SURFACE AND VELOCITY COMPARISONS .....	44

## LIST OF TABLES

Table 1:	Summary of six pile fence tests.....	5
----------	--------------------------------------	---

## LIST OF FIGURES

Figure 1:	Experimental setup for pile fence test. ....	4
Figure 2:	Double-row pile fence of DW test located at $x_p = 19.12$ m with dowels of diameter $b$ and spacing $S$ . ....	6
Figure 3:	Measured initial, intermediate, and final profiles for six tests. ....	9
Figure 4:	Measured temporal variations of wave overtopping rate $q_o$ and sand overwash rate $q_{bs}$ for DN, SN, DW, SW, and HB (bare dune) tests. ....	12
Figure 5:	Measured temporal variations of $q_o$ , $q_{bs}$ , and porosity $\varepsilon$ for toppling TD and TB tests. ....	13
Figure 6:	Measured and computed intermediate and final profiles for six tests. ....	19
Figure 7:	Measured and computed temporal variations of $q_o$ and $q_{bs}$ for six tests. ....	20
Figure 8:	Measured and computed cross-shore variations of free surface elevation $\eta_e$ and onshore velocity $U_e$ with exceedance probability $e = 5\%$ , $1\%$ , and $0.013\%$ for DN test. ....	22
Figure 9:	Correlation of measured and computed $\eta_e$ and $U_e$ with $e = 5\%$ , $1\%$ , and $0.013\%$ for six tests. ....	23
Figure A.1:	Initial (dotted black line), measured (solid black line), and computed (red line) profiles for the DN test. ....	28
Figure A.2:	Initial (dotted black line), measured (solid black line), and computed (red line) profiles for the SN test. ....	29
Figure A.3:	Initial (dotted black line), measured (solid black line), and computed (red line) profiles for the DW test. ....	29
Figure A.4:	Initial (dotted black line), measured (solid black line), and computed (red line) profiles for the SW test. ....	30

Figure A.5:	Initial (dotted black line), measured (solid black line), and computed (red line) profiles for the TD test. ....	30
Figure A.6:	Initial (dotted black line), measured (solid black line), and computed (red line) profiles for the TB test. ....	31
Figure B.1:	Measured and computed mean (top) and standard deviation (bottom) of the free surface elevation $\eta$ for the 17 runs of the DN test.....	32
Figure B.2:	Measured and computed mean (top) and standard deviation (bottom) of the cross-shore velocity $U$ for the 17 runs of the DN test.....	33
Figure B.3:	Measured and computed wet probability $P_w$ for the 17 runs of the DN test.....	33
Figure B.4:	Measured and computed mean (top) and standard deviation (bottom) of the free surface elevation $\eta$ for the 9 runs of the SN test.....	34
Figure B.5:	Measured and computed mean (top) and standard deviation (bottom) of the cross-shore velocity $U$ for the 9 runs of the SN test.....	35
Figure B.6:	Measured and computed wet probability $P_w$ for the 9 runs of the SN test. ....	35
Figure B.7:	Measured and computed mean (top) and standard deviation (bottom) of the free surface elevation $\eta$ for the 7 runs of the DW test.....	36
Figure B.8:	Measured and computed mean (top) and standard deviation (bottom) of the cross-shore velocity $U$ for the 7 runs of the DW test.....	37
Figure B.9:	Measured and computed wet probability $P_w$ for the 7 runs of the DW test. ....	37
Figure B.10:	Measured and computed mean (top) and standard deviation (bottom) of the free surface elevation $\eta$ for the 6 runs of the SW test. ....	38

Figure B.11:	Measured and computed mean (top) and standard deviation (bottom) of the cross-shore velocity $U$ for the 6 runs of the SW test. ....	39
Figure B.12:	Measured and computed wet probability $P_w$ for the 6 runs of the SW test.....	39
Figure B.13:	Measured and computed mean (top) and standard deviation (bottom) of the free surface elevation $\eta$ for the 11 runs of the TD test. ....	40
Figure B.14:	Measured and computed mean (top) and standard deviation (bottom) of the cross-shore velocity $U$ for the 11 runs of the TD test. ....	41
Figure B.15:	Measured and computed wet probability $P_w$ for the 11 runs of the TD test. ....	41
Figure B.16:	Measured and computed mean (top) and standard deviation (bottom) of the free surface elevation $\eta$ for the 8 runs of the TB test. ....	42
Figure B.17:	Measured and computed mean (top) and standard deviation (bottom) of the cross-shore velocity $U$ for the 8 runs of the TB test. ....	43
Figure B.18:	Measured and computed wet probability $P_w$ for the 8 runs of the TB test. ....	43
Figure C.1:	Measured and computed cross-shore variations of free surface elevation $\eta_e$ and onshore velocity $U_e$ with exceedance probability $e = 5\%$ , $1\%$ , and $0.013\%$ for DN test. ....	44
Figure C.2:	Measured and computed cross-shore variations of free surface elevation $\eta_e$ and onshore velocity $U_e$ with exceedance probability $e = 5\%$ , $1\%$ , and $0.013\%$ for SN test.....	45
Figure C.3:	Measured and computed cross-shore variations of free surface elevation $\eta_e$ and onshore velocity $U_e$ with exceedance probability $e = 5\%$ , $1\%$ , and $0.013\%$ for DW test. ....	45
Figure C.4:	Measured and computed cross-shore variations of free surface elevation $\eta_e$ and onshore velocity $U_e$ with exceedance probability $e = 5\%$ , $1\%$ , and $0.013\%$ for SW test.....	46

Figure C.5: Measured and computed cross-shore variations of free surface elevation  $\eta_e$  and onshore velocity  $U_e$  with exceedance probability  $e = 5\%$ ,  $1\%$ , and  $0.013\%$  for TD test. ....46

Figure C.6: Measured and computed cross-shore variations of free surface elevation  $\eta_e$  and onshore velocity  $U_e$  with exceedance probability  $e = 5\%$ ,  $1\%$ , and  $0.013\%$  for TB test.....47

## **ABSTRACT**

An experiment was performed to examine the utility of a pile fence in reducing dune erosion and overwash during a storm. Six tests consisting of 58 400-s runs were conducted to compare the effectiveness of six different pile fences. The limited experiment suggests that the pile fence with a porosity of about 0.5 should be placed near the toe of the dune foreslope with a sufficient burial depth to avoid toppling. A cross-shore numerical model is adjusted to simulate the drag force acting on the pile fence. The adjusted model is compared with the beach and dune profile evolution and the wave overtopping and sand overwash rates measured in the six tests. The model is expanded to predict the extreme (5%, 1%, and 0.013% exceedance probabilities) of the free surface elevation and onshore velocity for the future design of the pile fence against the wave forces. The proposed pile fence appears promising but will need to be tested at a field site.

## **Chapter 1**

### **INTRODUCTION**

A wide berm and a high dune can reduce coastal flooding damage caused by a severe storm but needs to be sustained by timely repair and periodic nourishment. The repair of the eroded berm and dune may not be possible if a subsequent storm occurs soon after the first storm. The sustainability of the wide berm and high dune will become more difficult if the mean sea level rise accelerates because of the greenhouse effect.

This study investigates the use of a permeable pile fence to reinforce a vulnerable dune against storms. The pile fence will also act as a wind fence to stabilize the dune against windblown sand transport. The traditional slat-type wind fence is not strong enough to withstand the wave force during a storm. The pile fence is intended to decrease the rate of dune erosion and crest lowering by reducing wave uprush, overtopping, and overwash. Coastal structures similar to the permeable pile fence include pile groins placed normal to the shoreline (Raudkivi 1996), vertical slotted barriers for reduction of transmitted waves (Isaacson et al. 1998), and pile row breakwaters placed parallel to the shoreline to restore an eroding beach (Reedijk and Muttray 2007). The pile fence will be placed parallel to the dune near its toe in the same manner as a wind fence.

An experiment was performed to quantify the effectiveness of a pile fence in reducing dune erosion and overwash where wooden dowels were used to represent piles. The profile evolution of a beach with a dune and the temporal changes of wave

overtopping and overwash rates were measured in six tests with different pile fence arrangements and locations without and with pile toppling. The six tests were compared to find the efficient arrangement and location of the pile fence. The cross-shore numerical model CSHORE (e.g. Figlus et al. 2011) is expanded to include the drag force acting on the pile fence. The expanded model is compared with the six tests. The following sections present the experiment, data analysis, numerical model, and comparison.

## **Chapter 2**

### **EXPERIMENT**

The experiment was conducted in the wave flume of the University of Delaware, which is 30 m long, 1.15 m wide, and 1.5 m high. Figure 1 depicts the experimental setup which is similar to the dune overwash experiment by Figlus et al. (2011) and the wooded dune experiment by Kobayashi et al. (2013). The sand beach in the flume consisted of well-sorted fine sand with a median diameter of 0.18 mm. The measured specific gravity, porosity, and fall velocity were 2.6, 0.4, and 2.0 cm/s, respectively. The piston-type wave maker in a 1-m depth generated a 400-s burst of irregular waves corresponding to a TMA spectrum. The spectral significant wave height and peak period were approximately 18 cm and 2.6 s, respectively. Eight capacitance wave gauges (WG1 – WG8) were used to measure the cross-shore and temporal variations of the free surface elevation above the still water level (SWL) where the vertical coordinate  $z$  is positive upward with  $z = 0$  at SWL. The most seaward WG1 was located in water depth of approximately 92 cm and its location is taken as the origin of the onshore coordinate  $x$ . Three acoustic Doppler velocimeters (V1 – V3) were used to measure fluid velocities at an elevation of 1/3 of the local water depth above the bottom.

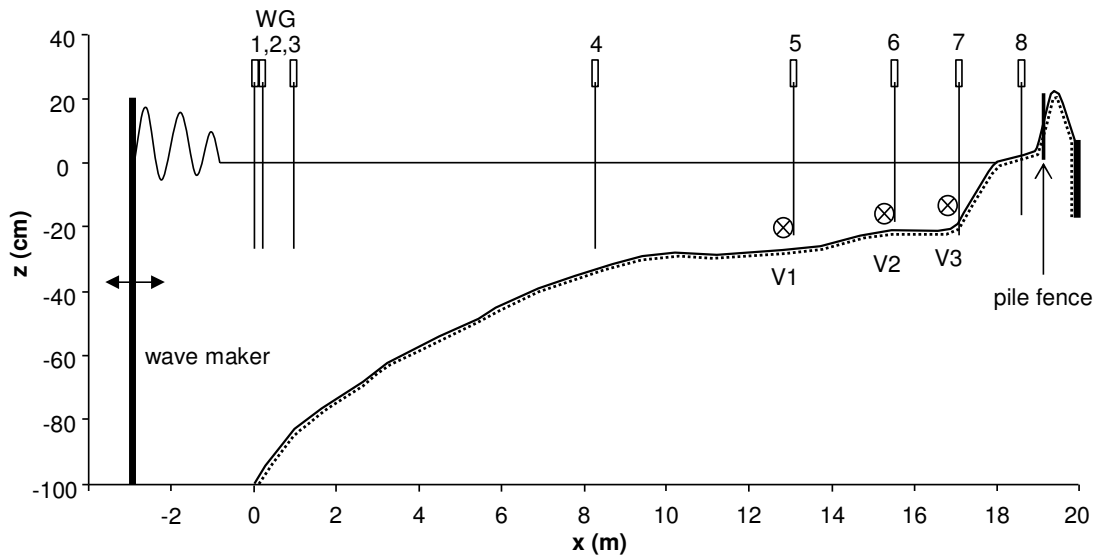


Figure 1: Experimental setup for pile fence test.

A laser line scanner and an array of three submerged ultrasonic transducers were used to measure the subaerial (after lowering the water level) and submerged portions of the bed, respectively. The measured bottom elevations were averaged alongshore to obtain the beach and dune profile  $z_b$  as a function of  $x$  at time  $t$  with  $t = 0$  at the beginning of each test. The initial berm and dune profile depicted in Figure 1 was the same for the six tests. The initial dune crest elevation was 21 cm above SWL and the foreslope and backslope of the dune were 1/2 to 1/3, respectively. The crest elevation of the vertical wall located at  $x = 19.9$  m was 6 cm above SWL. Water and sand transported over the vertical wall during each 400-s run were collected in a basin to measure the water overtopping rate and sand overwash rate averaged over the 400-s run. No nearshore bar was formed in this experiment.

Table 1 summarizes the six pile fence tests conducted in sequence. The number  $n$  of rows was  $n = 1$  (Single) or  $n = 2$  (Double). The diameter  $b$  of

cylindrical wooden dowels was  $b = 0.9$  cm. The dowel spacing  $S$  was  $S = 2$  cm (Narrow) or  $S = 4$  cm (Wide). The dowel length was 30 cm with a burial depth of 20 cm for the DN, SN, DW, and SW tests with the dowel height  $d = 10$  cm above the sand surface to ensure the emergence of the dowel top above uprushing water. The center of the pile fence for these four tests was at the cross-shore location  $x_p = 19.12$  m near the lower end of the dune foreslope in order to retard wave uprush on the upward slope. Figure 2 shows the staggered double-row pile fence of the DW test and its plan-view arrangement of the dowels. The dowel length for the Toppling tests TD and TB with  $n = 1$  and  $S = 2$  cm was 15 cm with the initial dowel height  $d = 5$  cm. During these two tests, the value of  $d$  was allowed to increase with the decrease of the 10-cm burial depth resulting from the berm and dune erosion. The pile fence was placed at  $x_p = 19.12$  m (Dune) for the TD test and moved to  $x_p = 18.64$  m (Berm) for the TB test where the berm and dune erosion was the minimum at  $x_p = 18.64$  m in the TD test.

Table 1: Summary of six pile fence tests.

Test	$n$	$S$ (cm)	$d$ (cm)	$x_p$ (m)	$\epsilon$	Number of runs
DN	2	2	10	19.12	0.10	17
SN	1	2	10	19.12	0.55	9
DW	2	4	10	19.12	0.55	7*
SW	1	4	10	19.12	0.78	6
TD	1	2	5	19.12	0.55	11
TB	1	2	5	18.64	0.55	8

\*DW test was terminated after 7 runs because of wave maker malfunction.

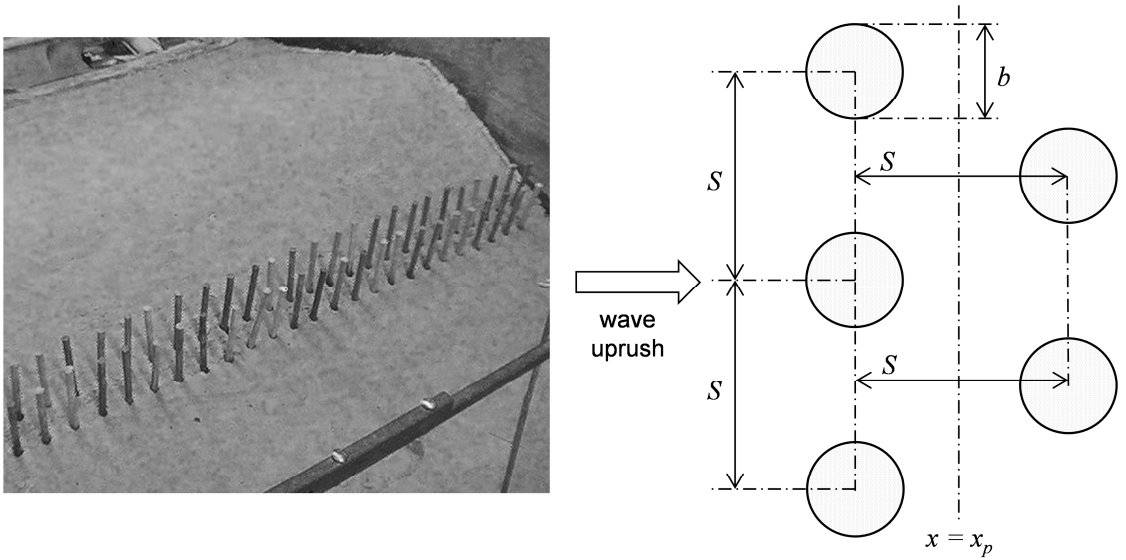


Figure 2: Double-row pile fence of DW test located at  $x_p = 19.12$  m with dowels of diameter  $b$  and spacing  $S$ .

The porosity  $\varepsilon$  listed in Table 1 is the fraction of alongshore opening encountered by wave uprush and downrush and given by

$$\varepsilon = (S - nb)/S \quad \text{for } n = 1 \text{ and } 2 \tag{1}$$

which assumes that the first and second rows for  $n = 2$  are equally effective because of the relatively small spacing  $S$  ( $S/b = 2.2 - 4.4$ ) between the two staggered rows. The porosities for the six tests were selected in light of the porosity of about 0.5 for wind fences recommended by the U.S. Army Corps of Engineers (2002). The number of 400-s runs conducted for each of the six runs is listed in Table 1. The tests were terminated when the dune crest was lowered to the elevation of the vertical wall crest or when the alongshore variability of the dune profile became excessive. The DW test was terminated at run 7 because of a wave maker malfunction during run 8. The porosity  $\varepsilon$  is found to be useful in assessing the effectiveness of the pile fence which is designed to reduce or slow dune erosion and overwash.

### Chapter 3

#### DATA ANALYSIS

The analyzed data presented in the report of Quan et al. (2014) are summarized in the following. The free surface elevation  $\eta$  above SWL was measured at WG1 – WG8 located at  $x = 0.0, 0.25, 0.95, 8.3, 12.9, 15.5, 17.1,$  and  $18.6$  m. WG1 – WG3 were outside the surf zone and WG4 was in the outer surf zone. WG5 – WG7 were in the inner surf zone and WG8 was in the swash zone. The fluid velocities were measured at V1 – V3 at  $x = 12.9, 15.5,$  and  $17.1$  m in the inner surf zone. The measured 400-s time series sampled at 20 Hz was reduced by removing the initial 20-s transition period before the data analysis. The analyzed time series consisted of 7600 data points. The time series from WG1 – WG3 were used to separate incident and reflected waves at the location of WG1. The incident spectral significant wave height  $H_{m0}$  and spectral peak period  $T_p$  were approximately 18 cm and 2.6 s, respectively. The reflection coefficient defined as the ratio between the values of  $H_{m0}$  for the reflected and incident waves was approximately 0.17 and the effect of the pile fence porosity was not detectable. The cross-shore variations of the mean  $\bar{\eta}$  and standard deviation  $\sigma_\eta$  of  $\eta$  at WG1 – WG8 were similar to those plotted in Kobayashi et al. (2013). The measured alongshore and vertical velocities were small in comparison to the cross-shore velocity  $U$ . The mean  $\bar{U}$  and standard deviation  $\sigma_U$  of  $U$  at V1 – V3 were also similar to those plotted in Kobayashi et al. (2013). The measured  $U$  is assumed to correspond to the depth-averaged velocity computed by the numerical

model. The effect of the pile fence porosity was not apparent in the values of  $\bar{\eta}$ ,  $\sigma_{\eta}$ ,  $\bar{U}$ , and  $\sigma_U$  measured seaward of the pile fence.

The beach and dune profiles measured after all the runs in each test were plotted together to examine the transition from dune foreslope erosion to dune overwash. Figure 3 shows the initial, intermediate, and final profiles in the zone of  $x = 15 - 19.9$  m of noticeable profile changes in front of the vertical wall. The location of the pile fence in each test is indicated in Figure 3 where the run number is affixed to the test name and the run number 0 corresponds to the initial profile. The berm and dune foreslope of the initial profile were eroded mostly by the seaward sand transport until the initial dune crest was lowered to the crest elevation of the intermediate profile. Wave overtopping and sand overwash increased rapidly with the acceleration of the dune crest lowering after the intermediate run in each test. For the DW test, the dune crest lowering from DW4 to DW7 was incomplete because of the wave maker malfunction during DW8.

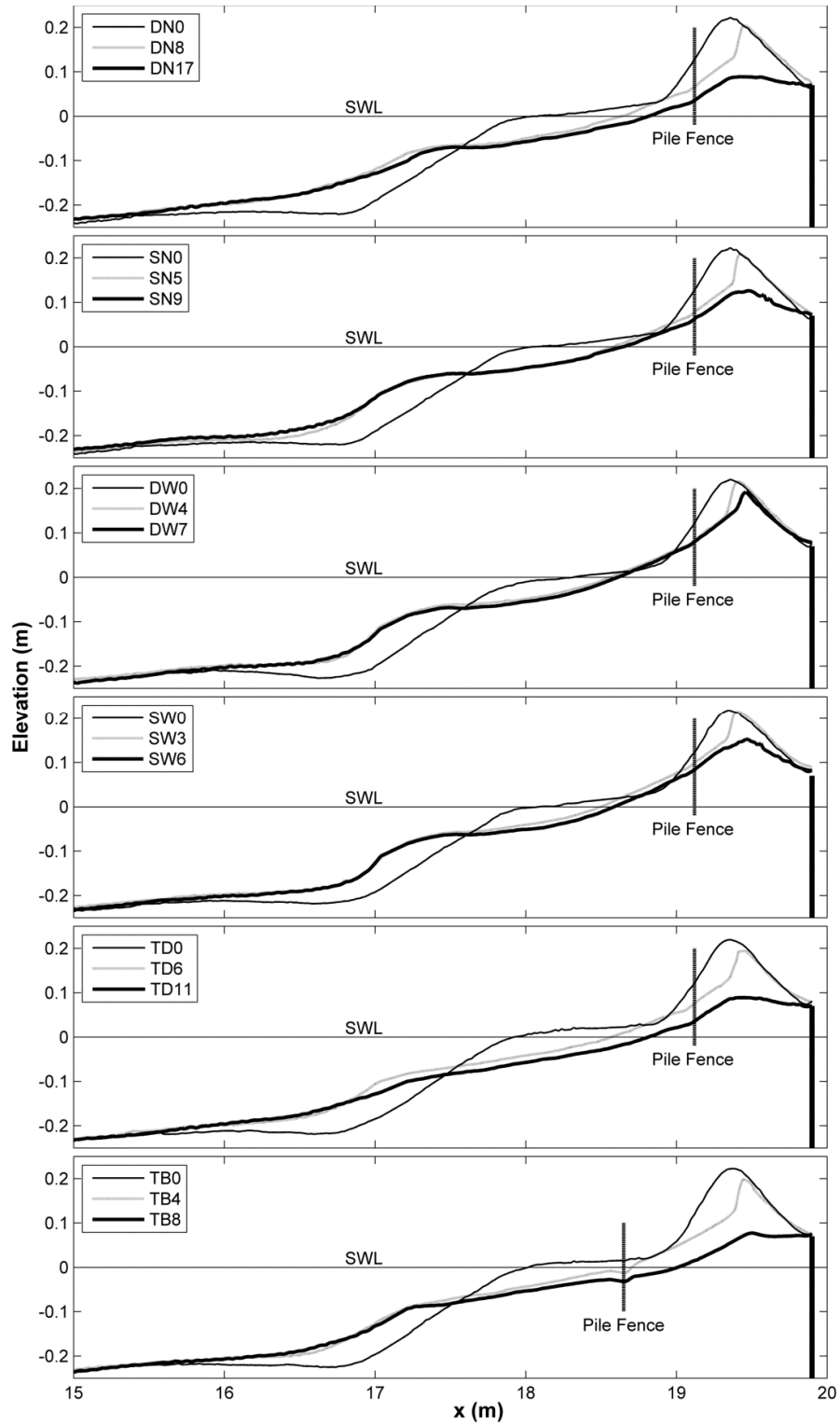


Figure 3: Measured initial, intermediate, and final profiles for six tests.

The comparisons of the DN ( $\varepsilon = 0.1$ ), SN ( $\varepsilon = 0.55$ ), DW ( $\varepsilon = 0.55$ ), and SW ( $\varepsilon = 0.78$ ) tests indicate the effect of the pile fence porosity on the retardation of the dune foreslope erosion and crest lowering. Wave uprush on the dune foreslope was observed to be reduced with the decrease of the porosity  $\varepsilon$ . The similarity between the SN (single row) and DW (double rows) tests with the same porosity is not very clear because the DW test was terminated before the sufficient lowering of the dune crest. The dune profile evolutions for the SN (no toppling) and TD (toppling) tests are similar because the short dowels in the TD test were not submerged during wave uprush. The TD test was continued longer to observe the dowel toppling during TD10 and TD11. The dowel toppling accelerated the dune crest lowering. The comparison between the TD and TB tests indicates the effect of the pile fence location. Local scour occurred in the vicinity of the pile fence on the berm in the TB test. The average dowel burial depth at the beginning of the toppling run was 2.2 cm for the dowels on the dune foreslope in the TD test and 5.7 cm for the dowels on the berm in the TB test. The larger water depth and onshore velocity on the berm caused the landward toppling of the dowels in the TB test which were submerged during large wave uprush. As a result, the pile fence on the berm was less effective in reducing the dune erosion and crest lowering.

The vertical wall at  $x = 19.9$  m may have influenced the eroded profile of the dune backslope but facilitated the measurement of the wave (water) overtopping rate  $q_o$  and sand overwash rate  $q_{bs}$ . Figure 4 shows the measured rates plotted at time  $t$  corresponding to the middle of each run for the DN, SN, DW, and SW tests. The values of  $q_o$  and  $q_{bs}$  were small during the transition from the initial profile to the intermediate profile which was caused mostly by the seaward sand transport. The

rapid increase of  $q_o$  and  $q_{bs}$  occurred after this transition and accelerated the dune crest lowering. The initial dune profile in this experiment was the same as that of the HB (high bare dune) test by Kobayashi et al. (2013). The measured  $q_o$  and  $q_{bs}$  for this test with  $\varepsilon = 1.0$  are plotted in Figure 4 to compare the temporal variations of  $q_o$  and  $q_{bs}$  for the five tests with  $\varepsilon = 0.1 - 1.0$ . The decrease of the porosity resulted in the delay of the rapid increase of  $q_o$  and  $q_{bs}$ . The temporal variations of  $q_o$  and  $q_{bs}$  for the SN and DW tests with  $\varepsilon = 0.55$  are similar until the early termination of the DW test. This indicates the validity of the porosity definition given by Eq. (1) for  $n = 1$  and 2. Fig. 4 indicates that the pile fence with the porosity of about 0.5 is effective in delaying the onset of the rapid increase of  $q_o$  and  $q_{bs}$ .

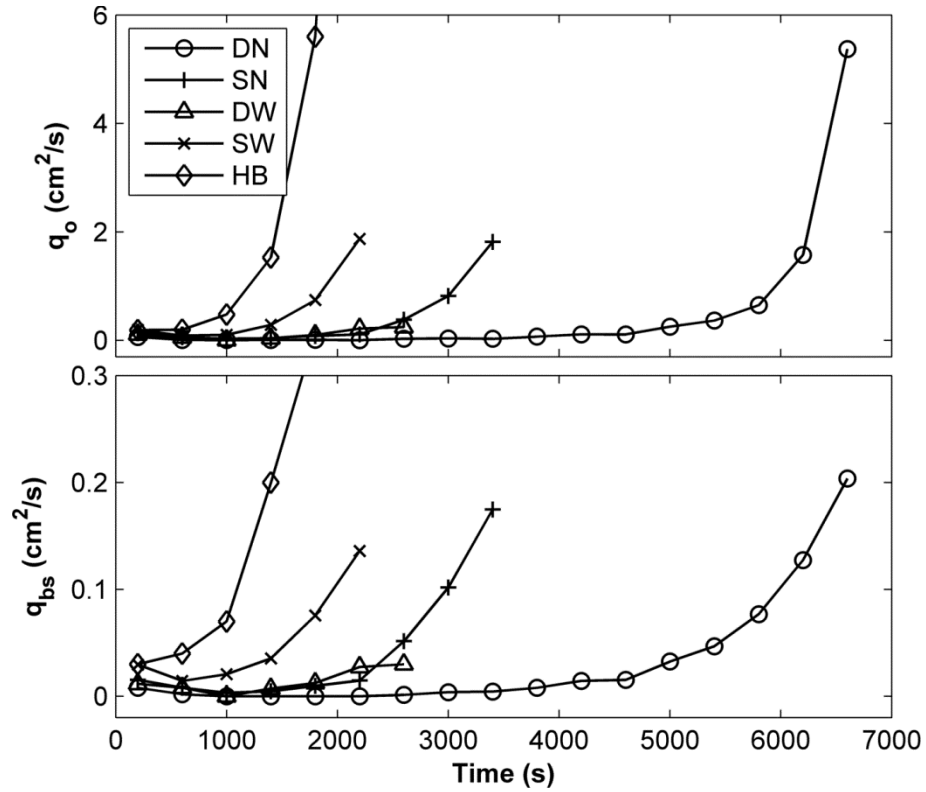


Figure 4: Measured temporal variations of wave overtopping rate  $q_o$  and sand overwash rate  $q_{bs}$  for DN, SN, DW, SW, and HB (bare dune) tests.

For the TD and TB tests, the dowel toppling increased the porosity from the initial value of  $\varepsilon = 0.55$ . The number of dowels placed alongshore was 58 at the beginning of these tests. The alongshore averaged porosity  $\varepsilon$  is calculated by assigning  $\varepsilon = 1.0$  for toppled dowels and  $\varepsilon = 0.55$  for intact dowels. Figure 5 shows the measured temporal variations of  $q_o$ ,  $q_{bs}$ , and  $\varepsilon$  for the TD and TB tests. These tests were continued until  $\varepsilon = 1.0$  and the final values of  $q_o$  and  $q_{bs}$  were larger than those shown in Figure 4. The onset of the dowel toppling occurred during the rapid increase of  $q_o$  and  $q_{bs}$  which resulted in the increased erosion in the zone near and landward of the pile fence. The pile fence placed near the lower end of the dune

foreslope was more stable because the water depth and onshore velocity of large wave uprush were observed to decrease landward. However, the wave force acting on the pile fence was not measured in this experiment.

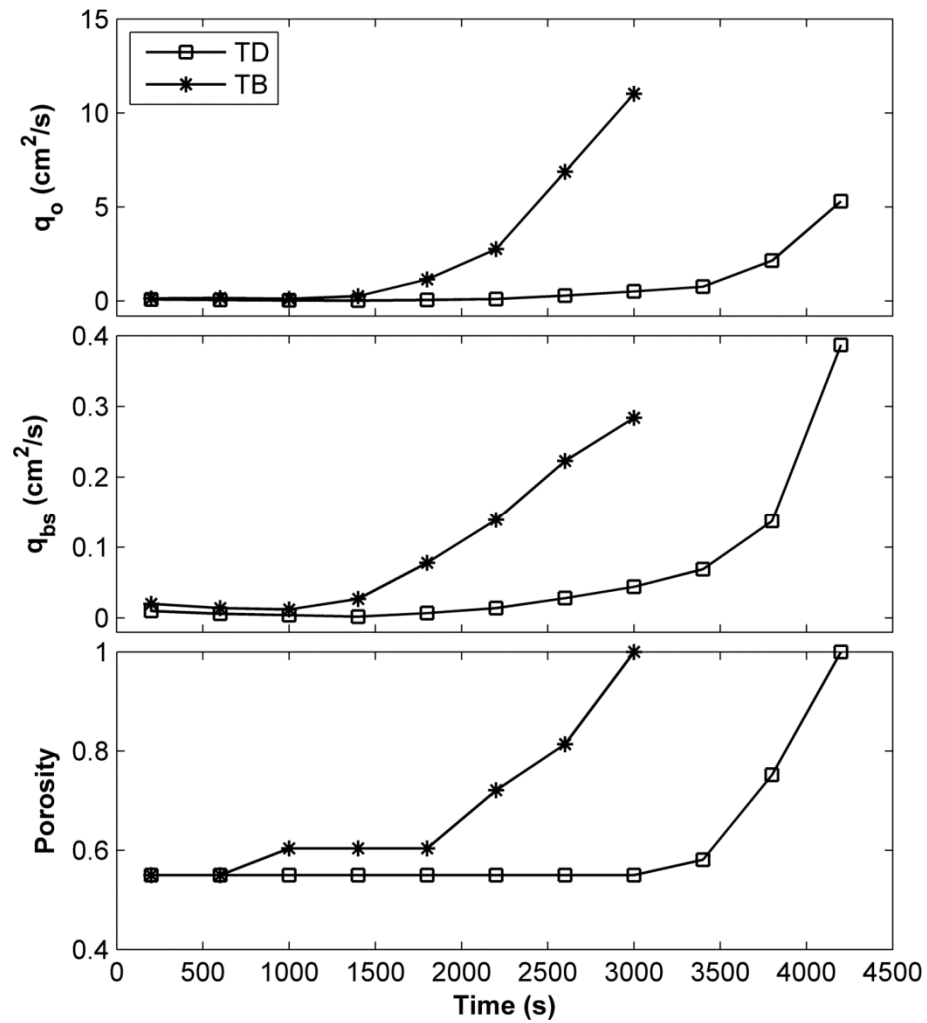


Figure 5: Measured temporal variations of  $q_o$ ,  $q_{bs}$ , and porosity  $\varepsilon$  for toppling TD and TB tests.

## Chapter 4

### NUMERICAL MODEL

A numerical model is required to generalize the findings of this small-scale experiment. The cross-shore model CSHORE has been compared with laboratory and field data on dune erosion and overwash (Figlus et al. 2011; Kobayashi and Jung 2012). This numerical model was expanded to predict wooded dune erosion and overwash (Ayat and Kobayashi 2014). This expanded model is shown to be applicable to the pile fence in the following. This numerical model based on the assumption of alongshore uniformity computes the cross-shore variations of  $\bar{\eta}$ ,  $\sigma_\eta$ ,  $\bar{U}$ , and  $\sigma_U$  using the time-averaged continuity, momentum, and energy equations. The increased flow resistance and energy dissipation caused by stems (dowels) are included in the expanded model. The time-averaged bed load and suspended sediment transport rates are computed using the formulas given by Figlus et al. (2011). The sediment transport rates are influenced by the stems through the hydrodynamic variables affected by the increased flow resistance and energy dissipation. If the landward-marching computation of the hydrodynamic variables and sediment transport rates reaches the landward end ( $x = 19.9$  m in the experiment), the wave overtopping rate  $q_o$  is calculated as the water volume flux per unit width, and the overwash rate  $q_{bs}$  is computed as the sum of the bed load and suspended sediment transport rates. The continuity equation of bottom sediment is used to compute the evolution of the bottom elevation  $z_b$ . The input parameters in the following computations are kept the same as those used by Ayat and Kobayashi (2014).

Ayat and Kobayashi (2014) expressed the instantaneous drag force  $\tau'_d$  acting on the dowels per unit horizontal area as

$$\tau'_d = \frac{1}{2} \rho C_D b N h_* |U|U \quad (2)$$

where  $\rho$  = fluid density;  $C_D$  = drag coefficient calibrated as  $C_D = 1.9$ ;  $b$  = width of each dowel normal to the cross-shore velocity  $U$ ;  $N$  = number of dowels per unit horizontal area; and  $h_*$  = submerged height of the dowel which equals the smaller value of the instantaneous water depth  $h = (\eta - z_b)$  and the dowel height  $d$  above the sand surface located at  $z = z_b$ . On the other hand, the instantaneous drag force  $f'_d$  acting on the pile fence per unit width may be expressed as

$$f'_d = \frac{1}{2} \rho C_D (1 - \varepsilon) h_* |U|U \quad (3)$$

where the porosity  $\varepsilon$  is given by Eq. (1). The drag force acting on each dowel is given by Eq. (3) with  $(1 - \varepsilon)$  replaced by the dowel width  $b$ .

The pile fence is located at  $x = x_p$ . The force  $f'_d$  per unit width may be approximated as the cumulative force of  $\tau'_d$  acting over a narrow strip of width  $(2W)$  in the zone of  $(x_p - W) \leq x \leq (x_p + W)$ . This approximation of  $f'_d = (2W\tau'_d)$  requires  $N = n/(2WS)$  in Eq. (2). The pile fence with given  $b$ ,  $n$ , and  $S$  is thus replaced by the dowel strip with the equivalent dowel density  $N$ . The cross-shore distance  $W$  is related to the constant nodal spacing  $\Delta x$  used in the numerical model. Use is made of  $\Delta x = 2$  cm and  $W = \Delta x$  in the following computations. The computed results with  $W = \Delta x$  and  $(2\Delta x)$  were found to be practically the same because the cumulative force  $f'_d$  in Eq. (3) is independent of  $W$ . The time-averaged drag force  $f_d$  per unit width is given by  $f_d = (2W\tau_d)$  with  $\tau_d$  = time-averaged drag force per unit

horizontal area. The analytical expressions for  $\tau_d$  were derived by Ayat and Kobayashi (2014).

The instantaneous water depth  $h = (\eta - z_b)$  and cross-shore velocity  $U$  are required to estimate the extreme wave force acting on each pile and the pile burial depth required against the extreme force. The numerical model predicts the cross-shore and temporal variations of  $\bar{\eta}$ ,  $\sigma_\eta$ ,  $\bar{U}$ ,  $\sigma_U$ , and  $z_b$  for the specified time series of  $H_{m0}$  and  $T_p$  at the seaward boundary  $x = 0$ . Saitoh and Kobayashi (2012) analyzed the extreme values of  $\eta$  and  $U$  measured on a semi-equilibrium beach in the wave flume used in the present experiment. Their data was limited to a single test consisting of seven 400-s runs. Their analysis is expanded using the six tests consisting of 58 runs in this experiment.

The extreme values of the measured  $\eta$  and  $U$  are obtained by ranking the 7600 measured values in each time series. The exceedance probability of the maximum value (first rank) is estimated to be 0.013%. The values exceeded by 5% and 1% of the 7600 values are also obtained. The values of  $\eta_e$  and  $U_e$  corresponding to the exceedance probability  $e$  are expressed in terms of the computed mean and standard deviation of  $\eta$  and  $U$

$$\eta_e = \bar{\eta} + C_e(1 + 0.4Q^{0.1})\sigma_\eta \quad \text{for } P_w > e \quad (4)$$

$$U_e = \bar{U} + C_e(1 + 0.1Q^{0.1})\sigma_U \quad \text{for } P_w > e \quad (5)$$

$$\text{with } e = 0.5\text{erfc}(C_e/\sqrt{2}) \quad (6)$$

where  $Q$  = fraction of irregular breaking waves;  $P_w$  = wet probability in the swash zone;  $\text{erfc}$  = complementary error function; and  $C_e$  = coefficient based on the Gaussian probability distribution with  $C_e = 1.64, 2.33$  and  $3.65$  for  $e = 5, 1,$  and  $0.013\%$ , respectively. The cross-shore variations of  $\bar{\eta}$ ,  $\sigma_\eta$ ,  $\bar{U}$ ,  $\sigma_U$ ,  $Q$ , and  $P_w$  are

computed by the numerical model. For nonbreaking waves ( $Q = 0$ ), Eqs. (4) and (5) become the same as those based on the Gaussian distribution. In the swash zone,  $Q = 1$  and all waves are assumed breaking. In the wet zone ( $P_w = 1$ ),  $P_w > e$  is satisfied. In the swash zone ( $P_w < 1$ ), the upper limit of  $e$  is imposed by  $P_w$  which is the ratio between the wet and total (wet and dry) durations. The effect of  $Q$  is smaller in Eq. (5) because  $U$  was measured at the elevation of  $1/3$  of the local water depth above the bottom. The measured and computed values of  $\eta_e$  and  $U_e$  are compared in the next section.

## **Chapter 5**

### **COMPARISON OF MODEL WITH MEASURED DATA**

The numerical model adjusted for the pile fence is compared with the six tests listed in Table 1. The measured and computed profiles are compared for all the runs in each test as presented in Appendix A. The comparisons for the intermediate and final profiles shown in Figure 3 represent the degree of agreement for each test. Figure 6 compares the measured and computed intermediate and final profiles for the six tests. The agreement for the six tests is similar to the previous comparisons by Figlus et al. (2011) with their bare dune tests and by Ayat and Kobayashi (2014) with their wooded dune tests. The scarped foreslope of the intermediate profile is not predicted adequately. The dune crest elevation of the final profile is not predicted accurately for all the tests. The average burial depths for the pile toppling for the TD and TB tests were 2.2 and 5.7 cm, respectively. These measured burial depths are specified as toppling criteria of these tests. The computed burial depths are 6 and 7 cm for the TD and TB tests, respectively. Consequently, the computed final profiles for the TD and TB tests do not include the pile toppling effect which increased the erosion of the measured final profile landward of the toppled pile fence.

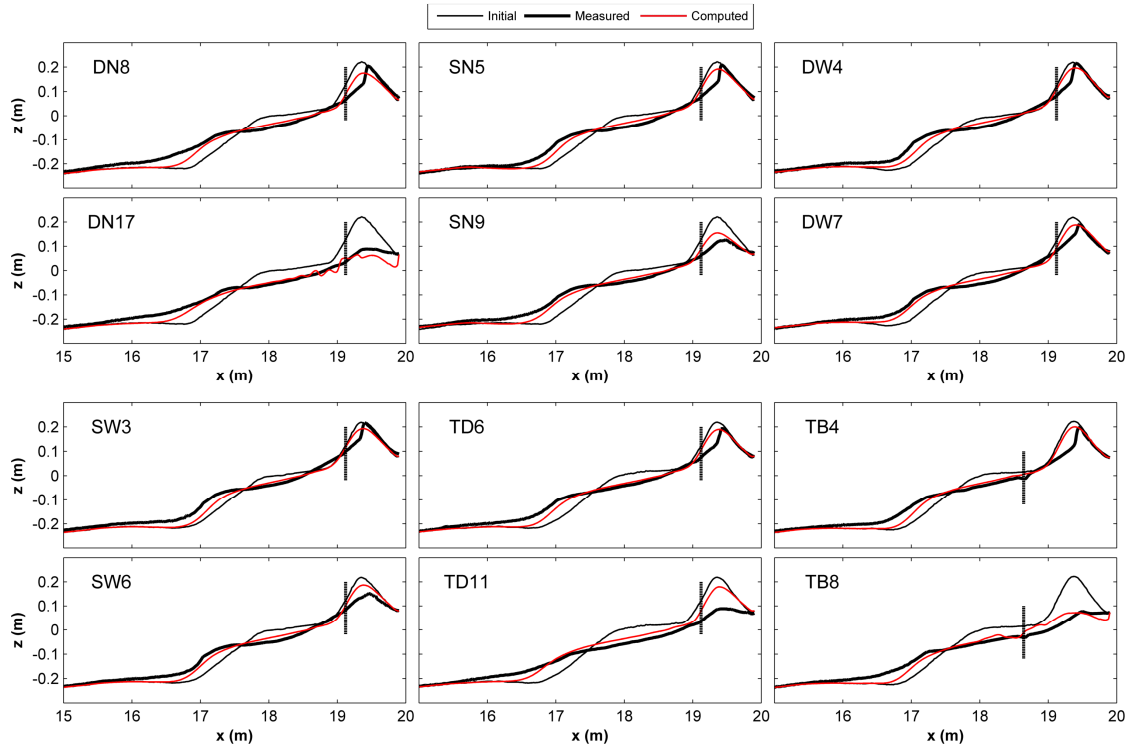


Figure 6: Measured and computed intermediate and final profiles for six tests.

Figure 7 compares the measured and computed time series of the wave overtopping rate  $q_o$  and sand overwash rate  $q_{bs}$ . The degree of agreement is similar to the previous comparisons by Figlus et al. (2011) and Ayat and Kobayashi (2014). The prediction accuracy of  $q_o$  and  $q_{bs}$  is affected by the accuracy of the predicted profile evolution in Figure 6. These rates resulting from intermittent wave overtopping events with very small water depths are difficult to predict accurately.

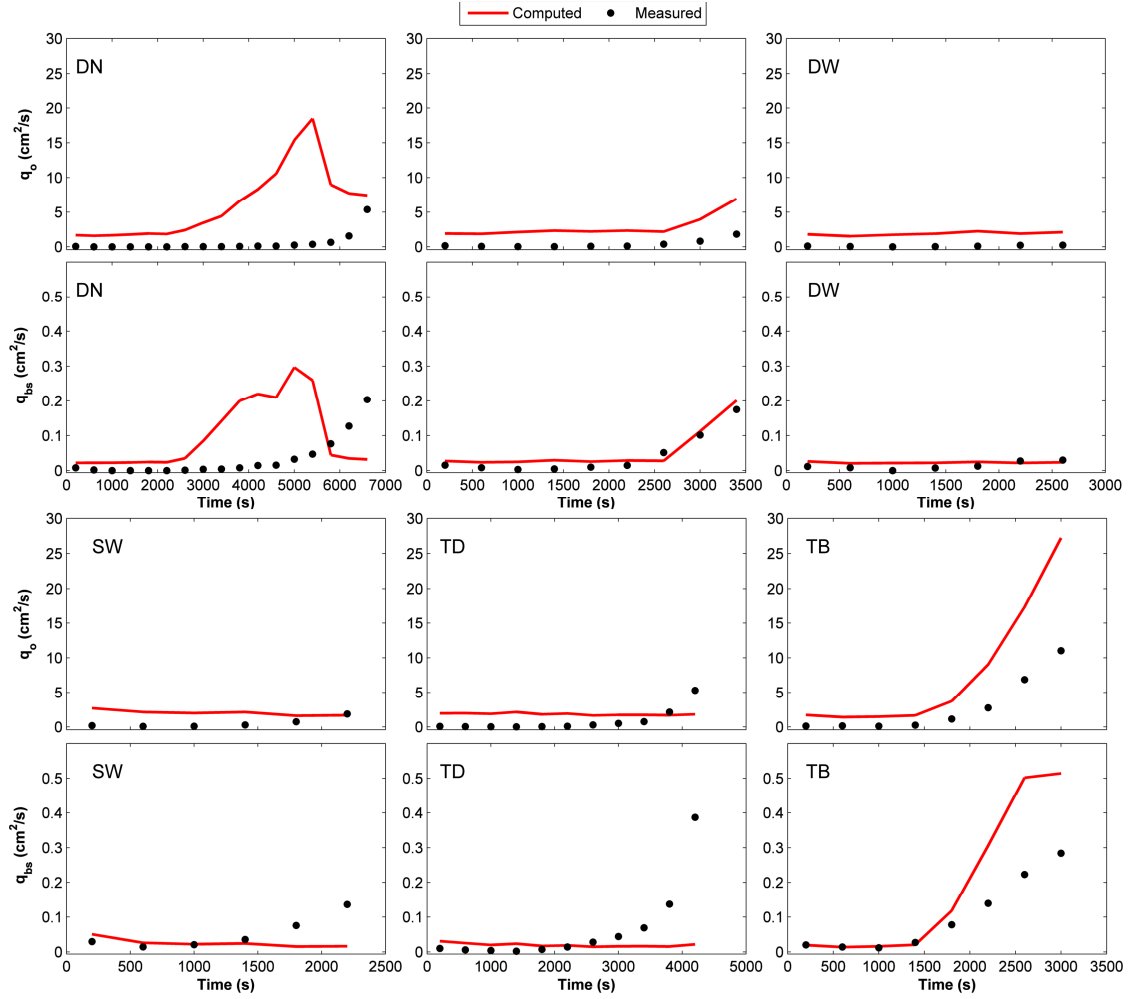


Figure 7: Measured and computed temporal variations of  $q_o$  and  $q_{bs}$  for six tests.

The measured and computed cross-shore variations of  $\bar{\eta}$ ,  $\sigma_\eta$ ,  $\bar{U}$ ,  $\sigma_U$ , and  $P_w$  are compared for all the runs in each test as presented in Appendix B. These hydrodynamic variables are predicted within errors of about 20% as in the previous comparisons. This apparent accuracy is related to the measurements of  $\eta$  and  $U$  which were conducted in the wet and lower swash zones with  $P_w = 0.9 - 1.0$ . The prediction

accuracy is expected to be lower in the zone of  $P_w < 0.9$  in view of the comparisons in Figure 7.

The measured and computed cross-shore variations of  $\eta_{5\%}$ ,  $\eta_{1\%}$ ,  $\eta_{max}$ ,  $U_{5\%}$ ,  $U_{1\%}$ , and  $U_{max}$  are also compared for all the runs in each test, as presented in Appendix C, where  $\eta_{max}$  and  $U_{max}$  are computed using Eqs. (4) and (5) with  $e = 0.013\%$ . Figure 8 shows the compared cross-shore variations for the DN test as examples. The measured and computed values for all the runs are plotted together. The computed cross-shore variations are almost the same for all the runs except in the dune erosion zone in front of the vertical wall. The data variability is relatively large for the maximum values. The computed  $\eta_{5\%}$ ,  $\eta_{1\%}$ , and  $\eta_{max}$  decrease with the lowering of the eroded dune crest because  $\eta = (h + z_b)$  is affected more by the bottom elevation  $z_b$  than the water depth  $h$  on the dune. The landward limit of the computed variation is imposed by the requirement of  $P_w > e$  in Eqs. (4) and (5). The computed  $U_{5\%}$ ,  $U_{1\%}$ , and  $U_{max}$  in the dune zone tend to increase with the dune crest lowering. The pile fences of the TD and TB tests were located at  $x = 19.12$  and  $18.64$  m, respectively. The computed onshore velocities, which are similar to those in Figure 8, are larger at  $x = 18.64$  m than  $x = 19.12$  m. This may explain the earlier pile toppling in the TB test.

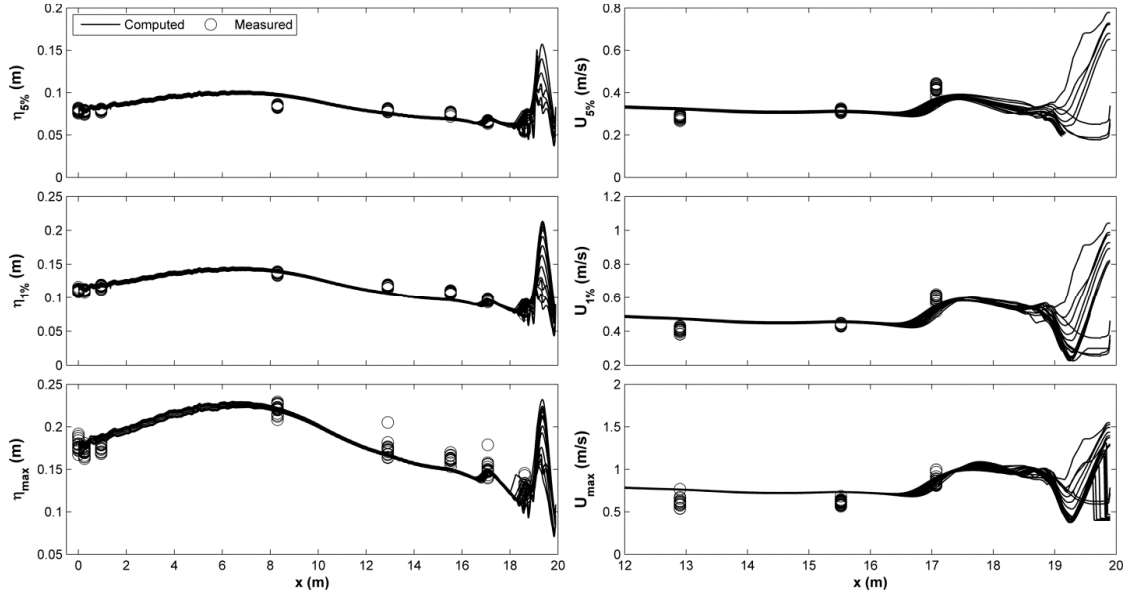


Figure 8: Measured and computed cross-shore variations of free surface elevation  $\eta_e$  and onshore velocity  $U_e$  with exceedance probability  $e = 5\%$ ,  $1\%$ , and  $0.013\%$  for DN test.

The measured and computed values of  $\eta_{5\%}$ ,  $\eta_{1\%}$ ,  $\eta_{max}$ ,  $U_{5\%}$ ,  $U_{1\%}$ , and  $U_{max}$  for the six tests are compared in Figure 9. The perfect agreement and deviations of  $\pm 20\%$  are indicated by a solid line and two dashed lines. The correlation coefficient  $R$  is also given for each comparison. The numerical model predicts these extreme values mostly within errors of 20% partly because Eqs. (4) and (5) are calibrated using these six tests. Eqs. (4) and (5) will need to be verified using additional data sets. The verified equations will allow us to assess coastal flooding damage in more rational manners than the existing methods described in Coastal Construction Manual (U.S. Department of Homeland Security, Federal Emergency Management Agency 2011).

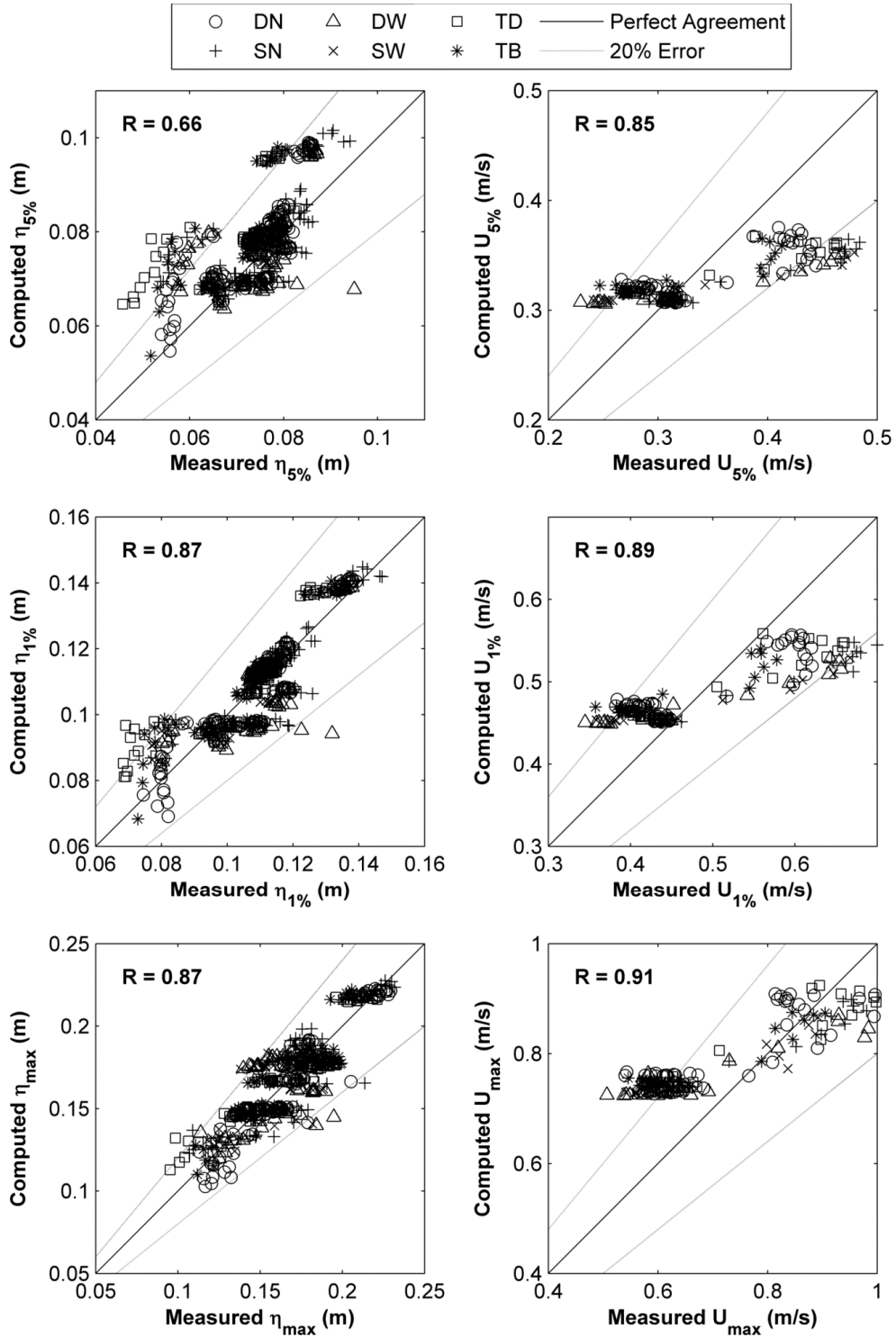


Figure 9: Correlation of measured and computed  $\eta_e$  and  $U_e$  with  $e = 5\%$ ,  $1\%$ , and  $0.013\%$  for six tests.

## **Chapter 6**

### **CONCLUSIONS**

An experiment was performed to examine the utility of a pile fence in reducing dune erosion and overwash during a storm. Six tests consisting of 58 400-s runs were conducted to compare the effectiveness of six different pile fences. The design variables examined in the six tests were the pile spacing, number of rows (single or staggered double), fence location (dune foreslope or berm), and pile length and toppling. The effects of the pile spacing and number of rows were combined and expressed using the pile fence porosity which is the fraction of alongshore opening encountered by wave uprush and downrush. The pile fence was observed to be effective in reducing wave uprush and overtopping and delaying dune erosion and overwash. The efficiency of the pile fence was shown to increase with the decrease of its porosity. The pile fence on the berm encountered a larger water depth and onshore velocity and was toppled landward earlier than the pile fence near the lower end of the dune foreslope. This limited experiment suggests that the pile fence with a porosity of about 0.5 should be placed near the toe of the dune foreslope with a sufficient burial depth to avoid toppling. The suggested porosity and location of the pile fence are consistent with those of a wind fence (U.S. Army Corps of Engineers 2002). As a result, the pile fence may also stabilize the dune against windblown sand transport under normal conditions.

The numerical model developed for the prediction of erosion and overwash of a wooded dune (Ayat and Kobayashi 2014) is adjusted to simulate the drag force

acting on the pile fence. The adjusted model is compared with the beach and dune profile evolution and the wave overtopping and sand overwash rates measured in the six tests. The overall agreement is reasonable but the accuracy is not consistent for all the tests. The numerical model predicts the mean and standard deviation of the free surface elevation and cross-shore velocity within errors of about 20%. Simple formulas are proposed to predict the extreme values of the free surface elevation and onshore velocity required for the design of the pile fence against the wave force. The numerical model coupled with the formulas is shown to predict the free surface elevations and onshore velocities with 5%, 1%, and 0.013% exceedance probabilities within similar accuracy.

The proposed pile fence will need to be tested at a field site in the future. A possible site may be a developed beach that is too narrow to build a high and wide dune against a severe storm. The pile fence may also be applied to reinforce a weak spot or gap of an existing dune.

## REFERENCES

- Ayat, B., and Kobayashi, N. (2014). "Vertical cylinder density and toppling effects on dune erosion and overwash." *J. Waterway, Port, Coastal, Ocean Eng.*, (in press).
- Figlus, J., Kobayashi, N., Gralher, C., and Iranzo, V. (2011). "Wave overtopping and overwash of dunes." *J. Waterway, Port, Coastal, Ocean Eng.*, 137(1), 26-33.
- Isaacson, M., Premasiri, S., and Yang, G. (1998). "Wave interactions with vertical slotted barrier." *J. Waterway, Port, Coastal, Ocean Eng.*, 124(3), 118-126.
- Kobayashi, N., Gralher, C., and Do, K. (2013). "Effects of woody plants on dune erosion and overwash." *J. Waterway, Port, Coastal, Ocean Eng.*, 139(6), 466-472.
- Kobayashi, N., and Jung, H. (2012). "Beach erosion and recovery." *J. Waterway, Port, Coastal, Ocean Eng.*, 138(6), 473-483.
- Quan, R., Kobayashi, N., and Ayat, B. (2014). "Experiment on pile fence to enhance dune resiliency." Research Report No. CACR-14-03, Center for Applied Coastal Research, University of Delaware, Newark, Del.
- Raudkivi, A.J. (1996). "Permeable pile groins." *J. Waterway, Port, Coastal, Ocean Eng.*, 122(6), 267-272.
- Reedijk, B., and Muttray, M. (2007). "Pile row breakwaters at Langkawi, Malaysia, 10 years of beach development." *Proc. Coastal Structures 2007*, World Scientific, Singapore, 562-573.

- Saitoh, T., and Kobayashi, N. (2012). "Wave transformation and cross-shore sediment transport on sloping beach in front of vertical wall." *J. Coast. Res.*, 28(2), 354-359.
- U.S. Army Corps of Engineers. (2002). *Coast engineering manual, Engineer manual 1110-2-1100*, Washington, D.C.
- U.S. Department of Homeland Security, Federal Emergency Management Agency. (2011). *Coastal construction manual: Principles and practices of planning, siting, designing, constructing, and maintaining residential buildings in coastal areas*, 4th edition, FEMA P-55, Volume 1.

**Appendix A**  
**PROFILE COMPARISONS**

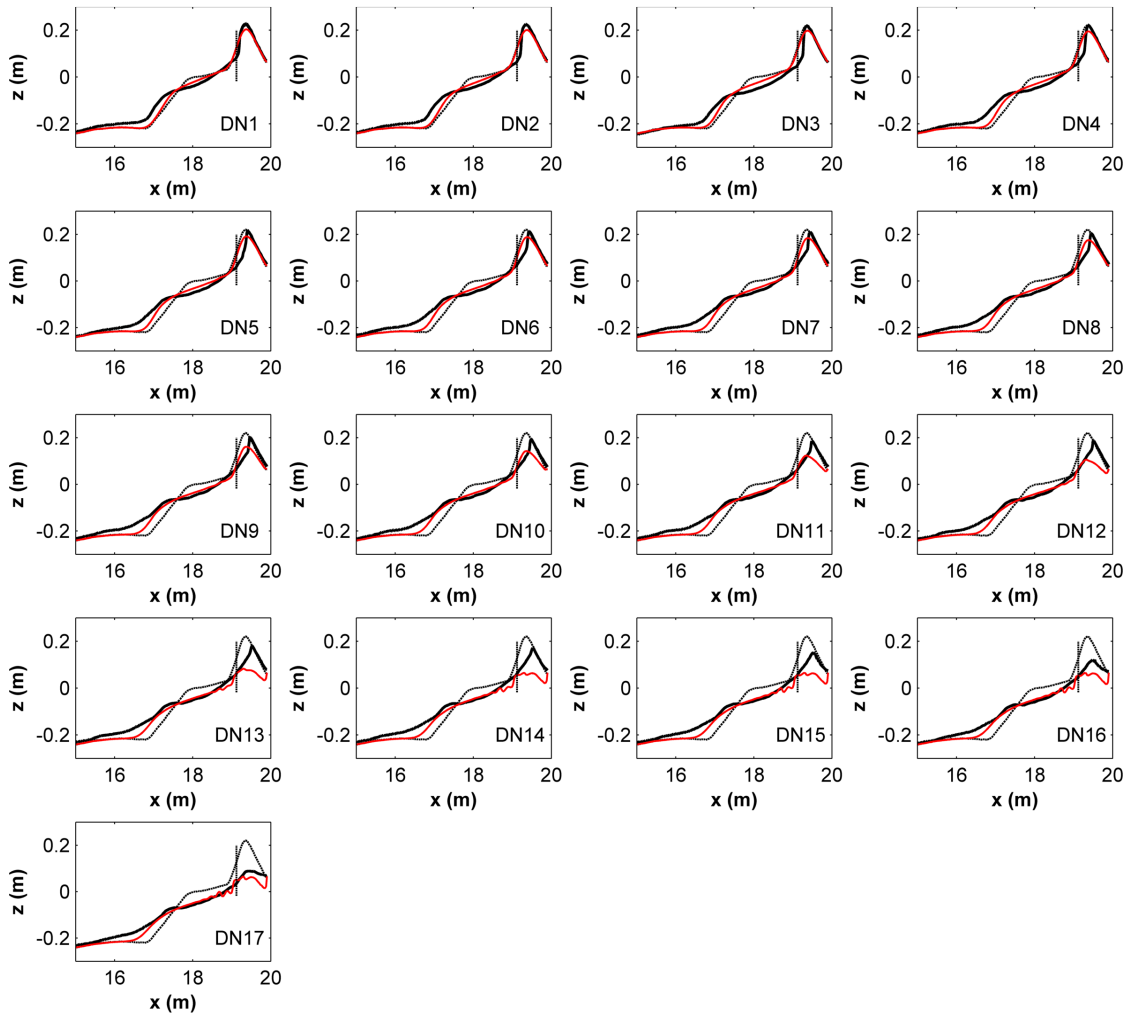


Figure A.1: Initial (thin black line), measured (thick black line), and computed (red line) profiles for the DN test.

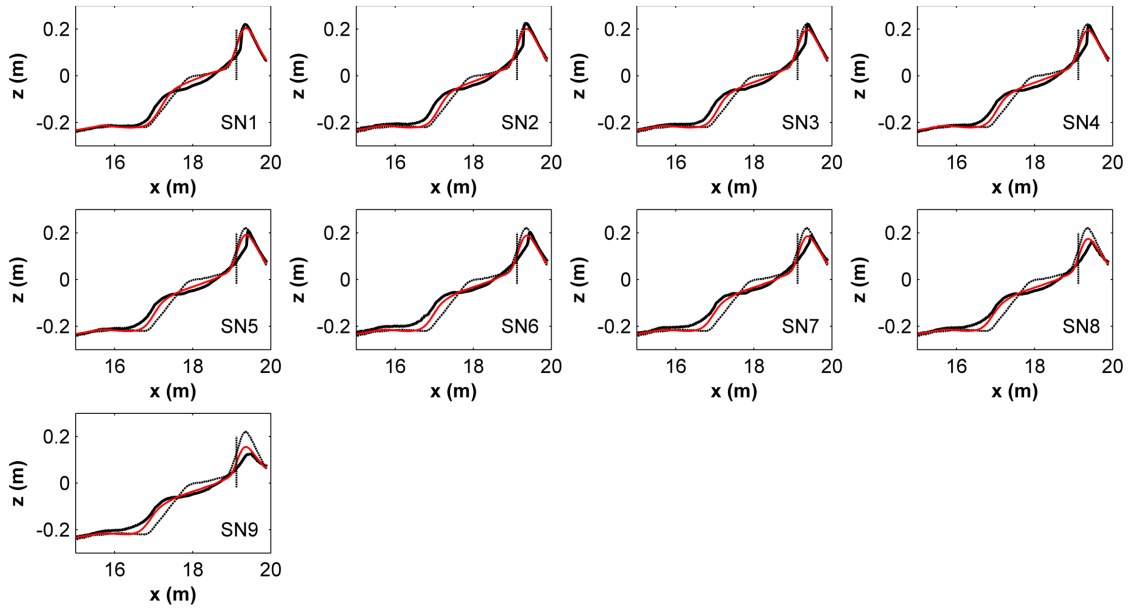


Figure A.2: Initial (thin black line), measured (thick black line), and computed (red line) profiles for the SN test.

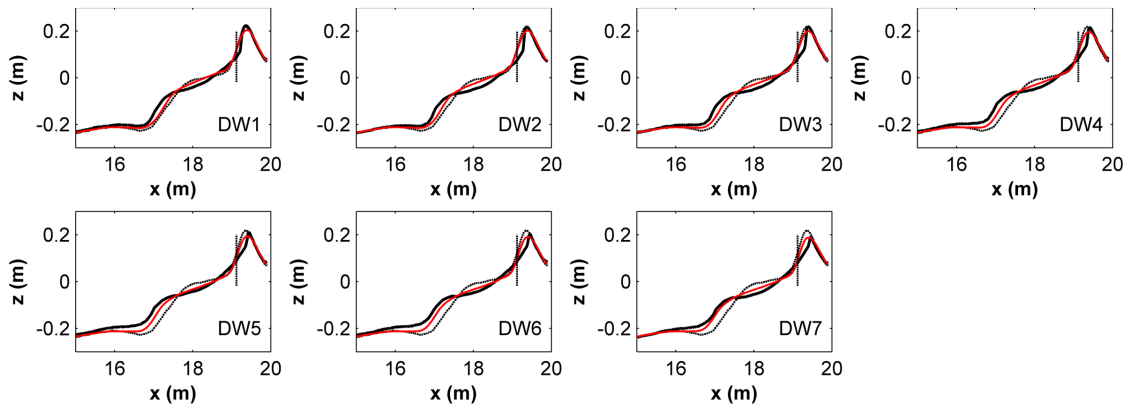


Figure A.3: Initial (thin black line), measured (thick black line), and computed (red line) profiles for the DW test.

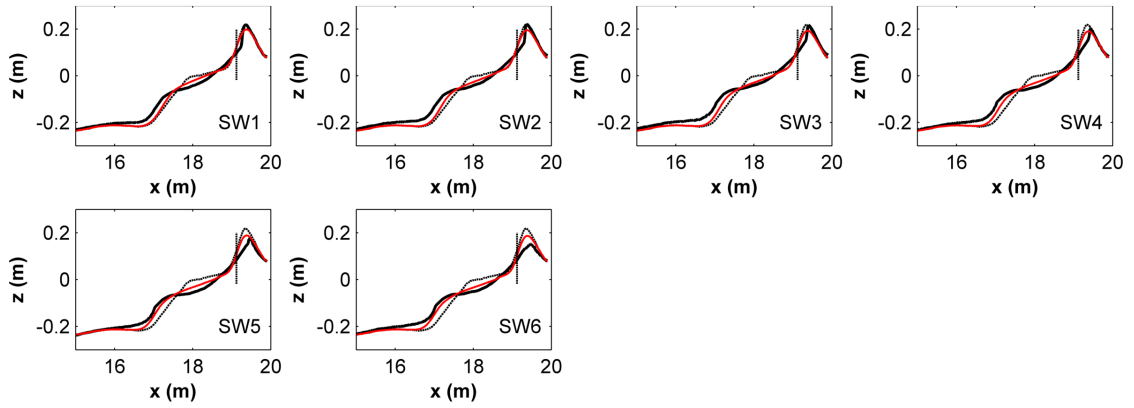


Figure A.4: Initial (thin black line), measured (thick black line), and computed (red line) profiles for the SW test.

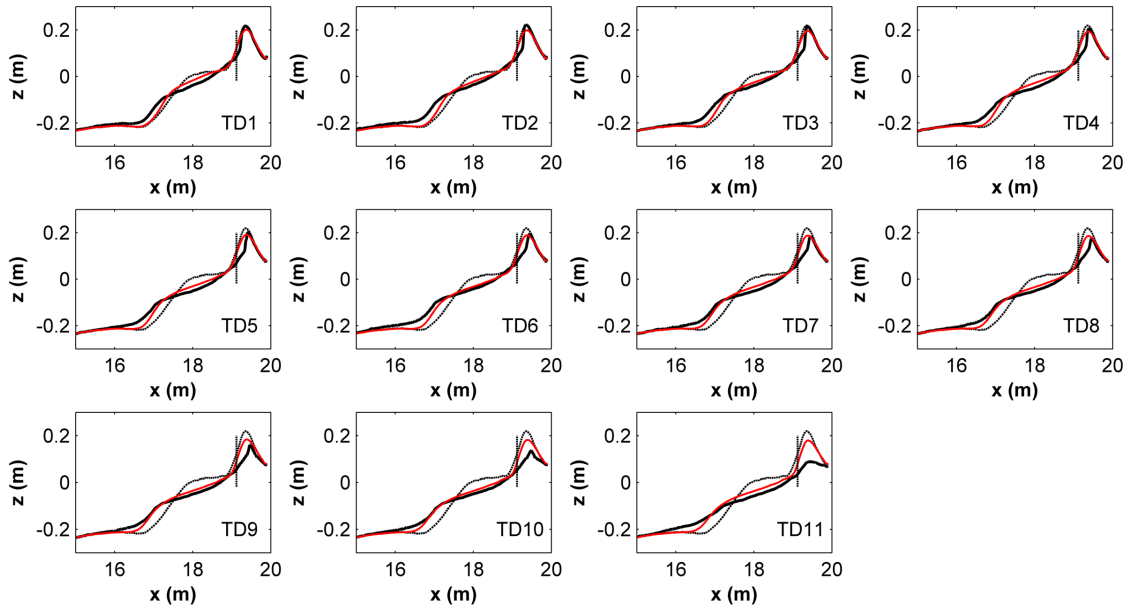


Figure A.5: Initial (thin black line), measured (thick black line), and computed (red line) profiles for the TD test.

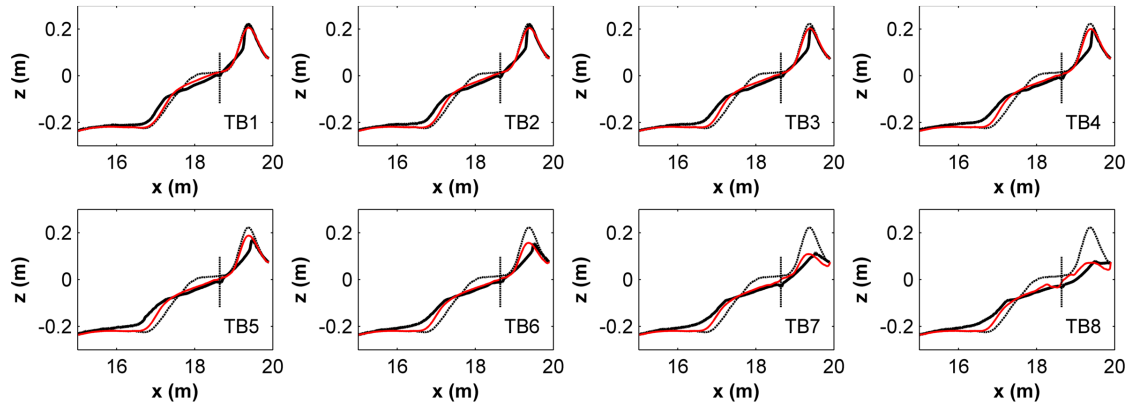


Figure A.6: Initial (thin black line), measured (thick black line), and computed (red line) profiles for the TB test.

## Appendix B

### FREE SURFACE, VELOCITY, AND WET PROBABILITY COMPARISONS

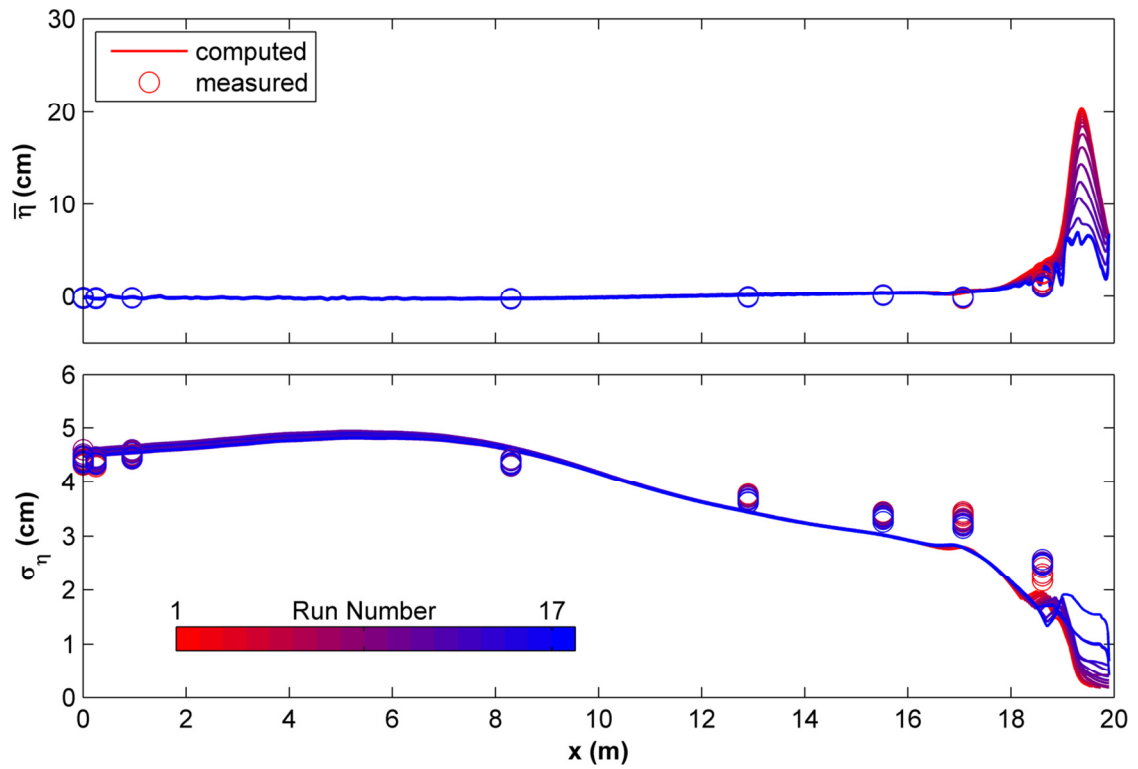


Figure B.1: Measured and computed mean (top) and standard deviation (bottom) of the free surface elevation  $\eta$  for the 17 runs of the DN test.

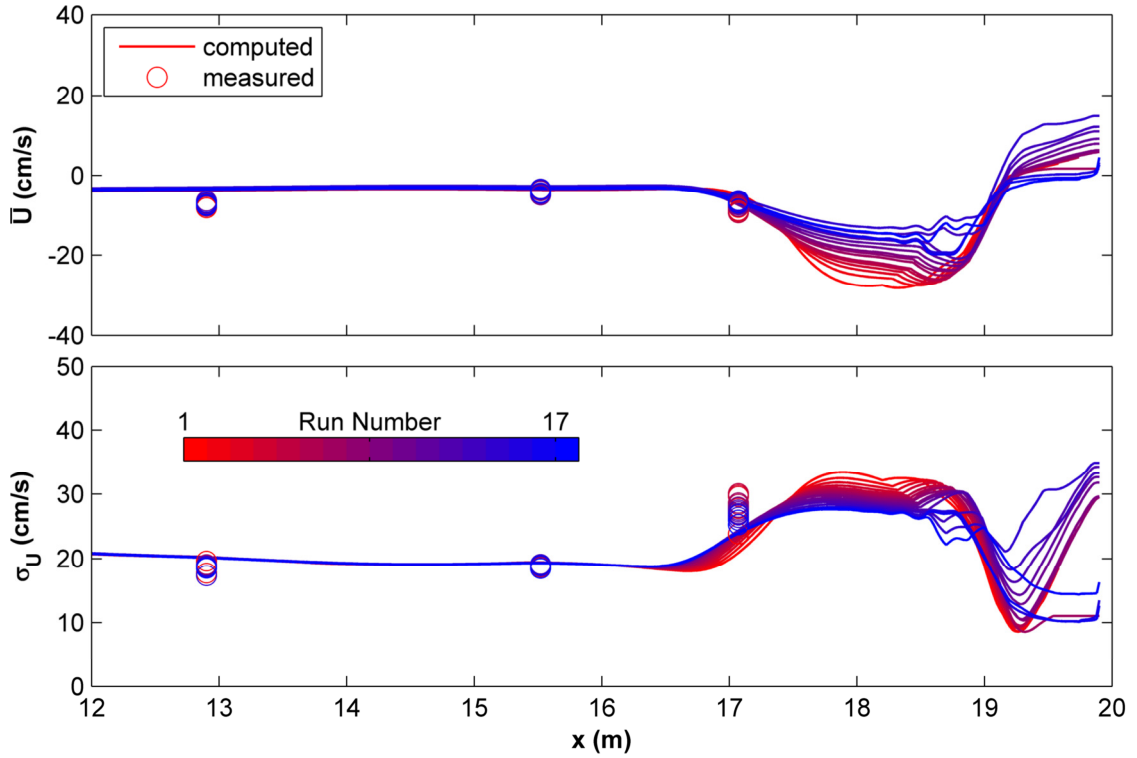


Figure B.2: Measured and computed mean (top) and standard deviation (bottom) of the cross-shore velocity  $U$  for the 17 runs of the DN test.

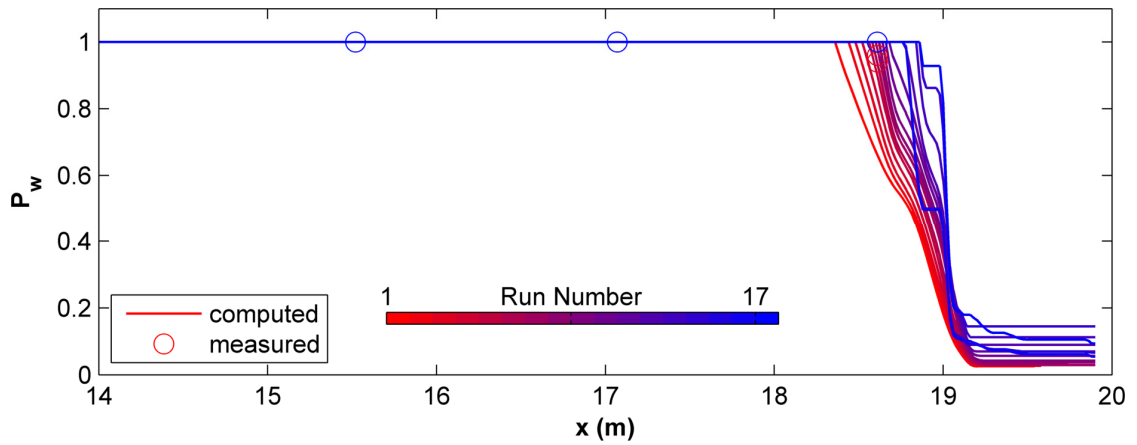


Figure B.3: Measured and computed wet probability  $P_w$  for the 17 runs of the DN test.

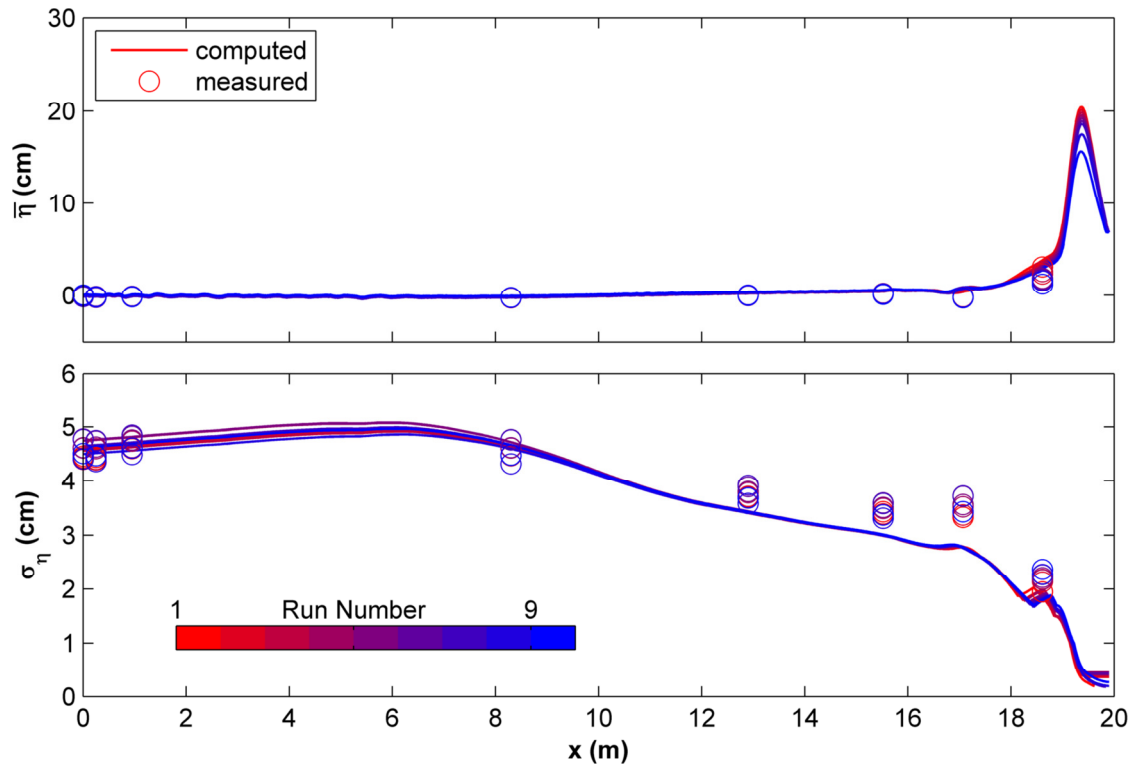


Figure B.4: Measured and computed mean (top) and standard deviation (bottom) of the free surface elevation  $\eta$  for the 9 runs of the SN test.

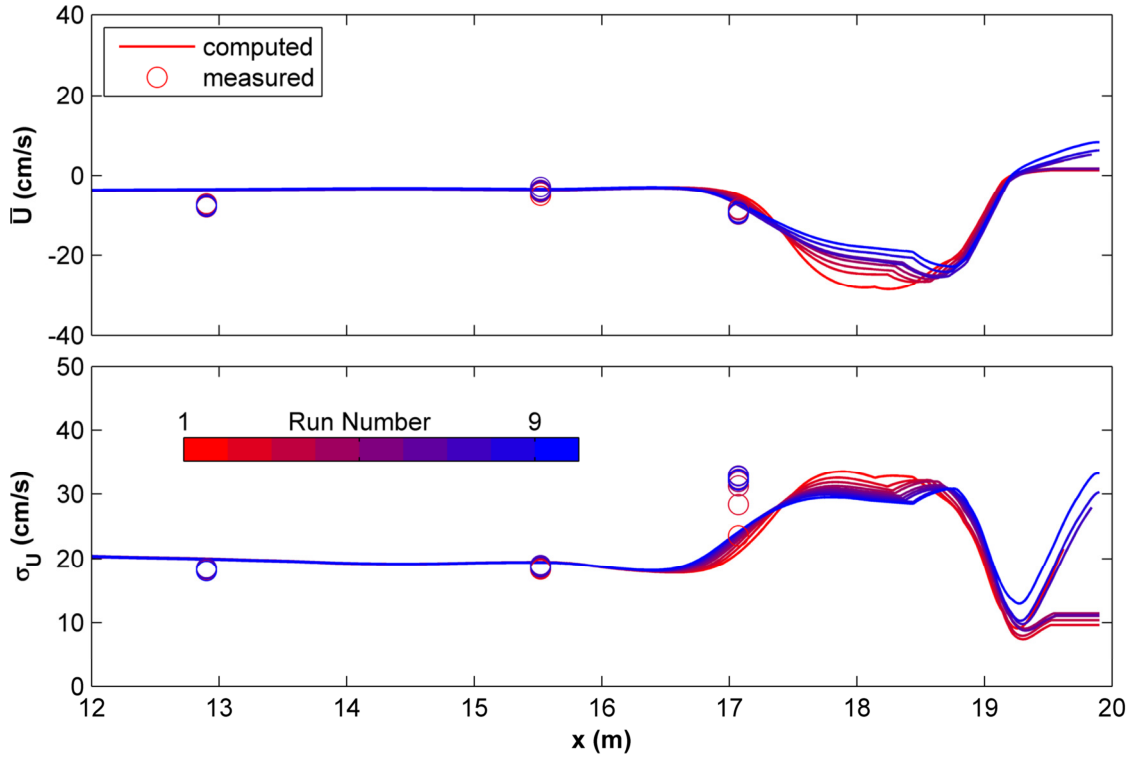


Figure B.5: Measured and computed mean (top) and standard deviation (bottom) of the cross-shore velocity  $U$  for the 9 runs of the SN test.

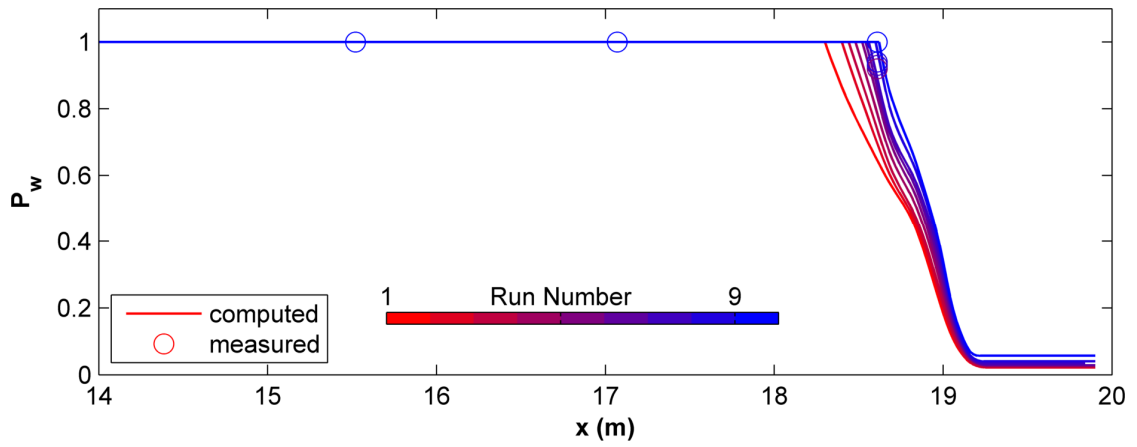


Figure B.6: Measured and computed wet probability  $P_w$  for the 9 runs of the SN test.

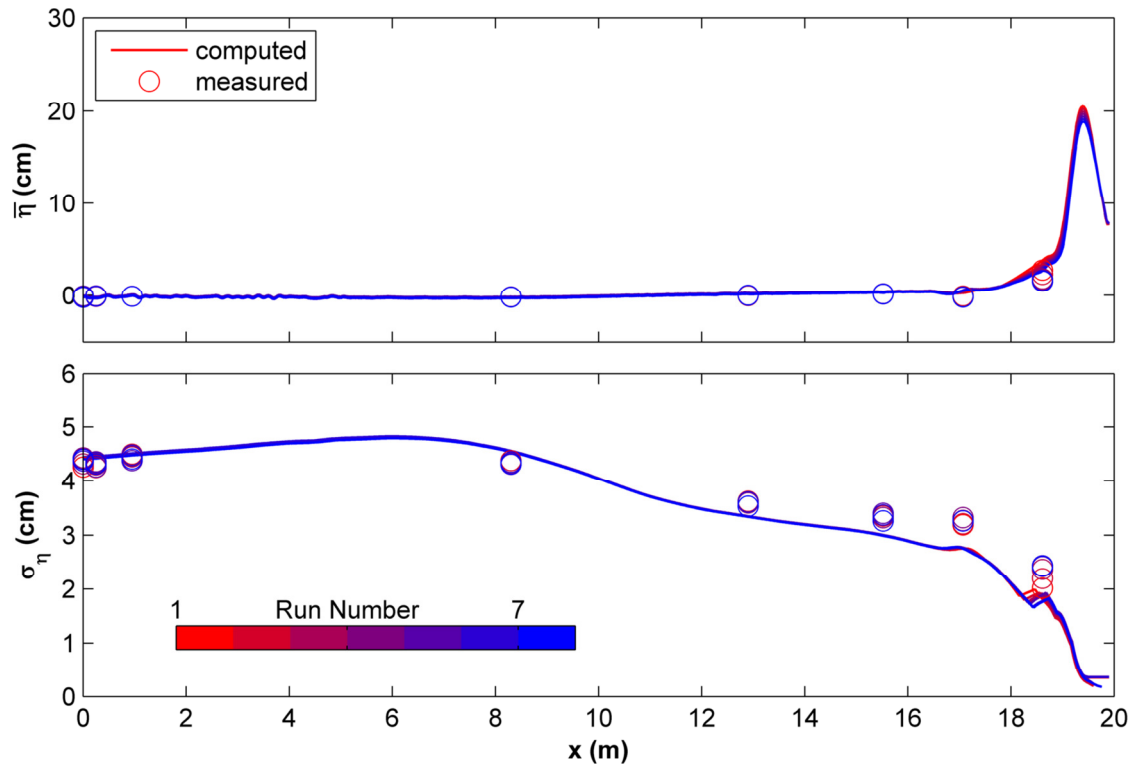


Figure B.7: Measured and computed mean (top) and standard deviation (bottom) of the free surface elevation  $\eta$  for the 7 runs of the DW test.

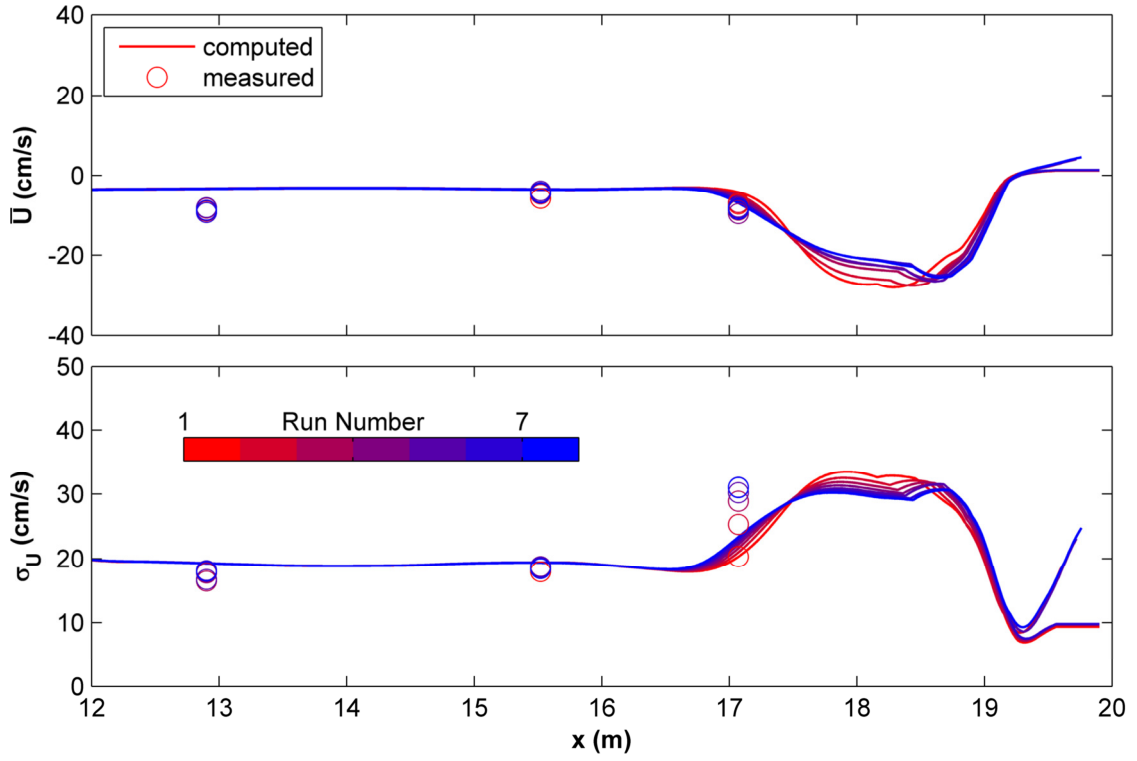


Figure B.8: Measured and computed mean (top) and standard deviation (bottom) of the cross-shore velocity  $U$  for the 7 runs of the DW test.

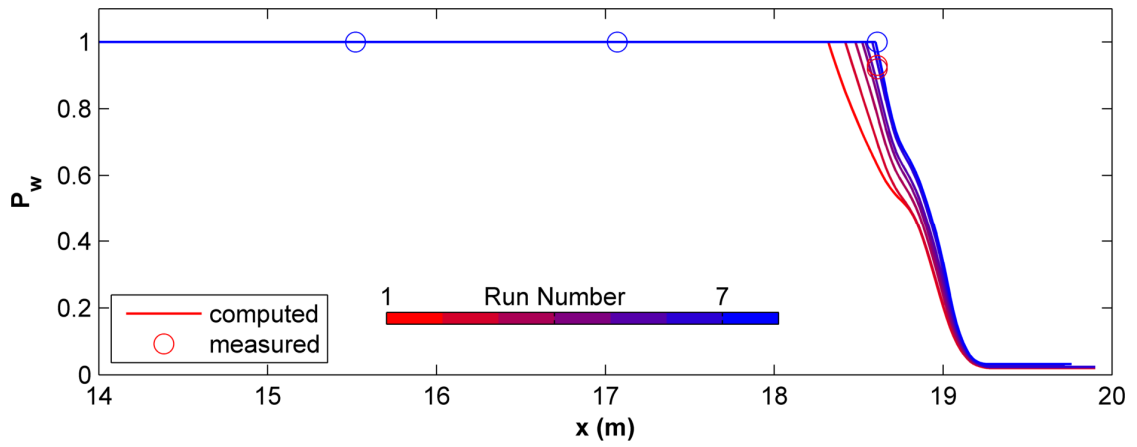


Figure B.9: Measured and computed wet probability  $P_w$  for the 7 runs of the DW test.

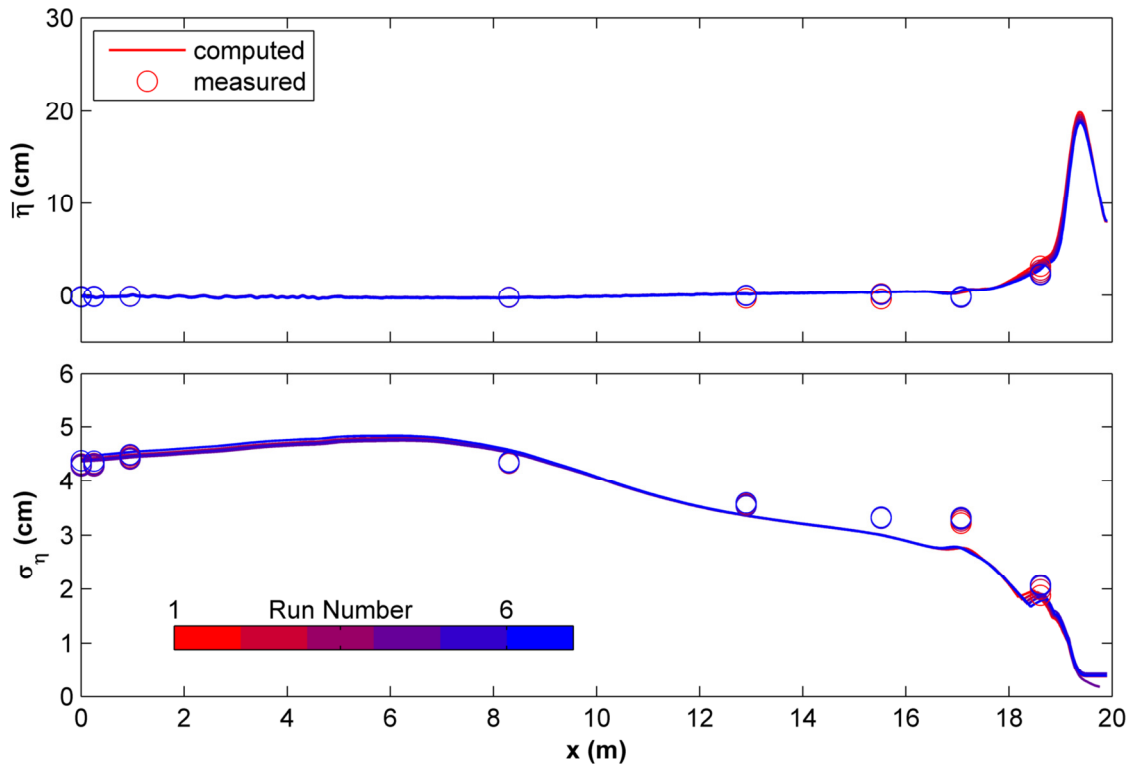


Figure B.10: Measured and computed mean (top) and standard deviation (bottom) of the free surface elevation  $\eta$  for the 6 runs of the SW test.

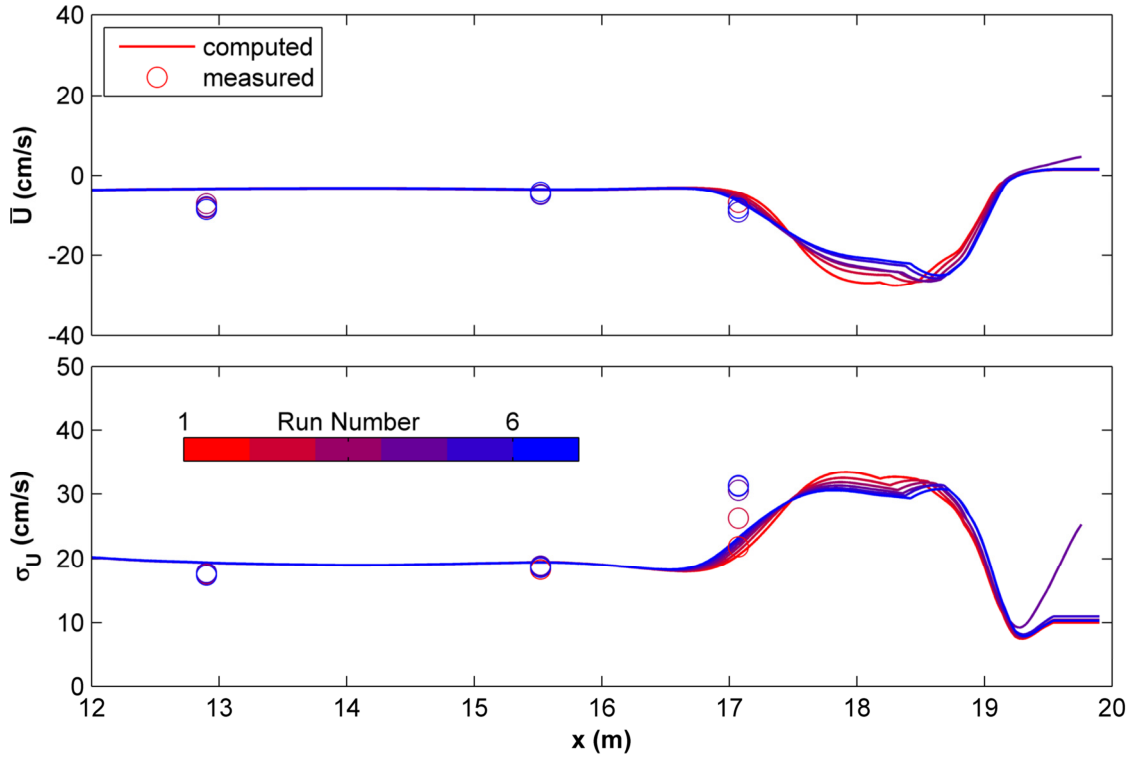


Figure B.11: Measured and computed mean (top) and standard deviation (bottom) of the cross-shore velocity  $U$  for the 6 runs of the SW test.

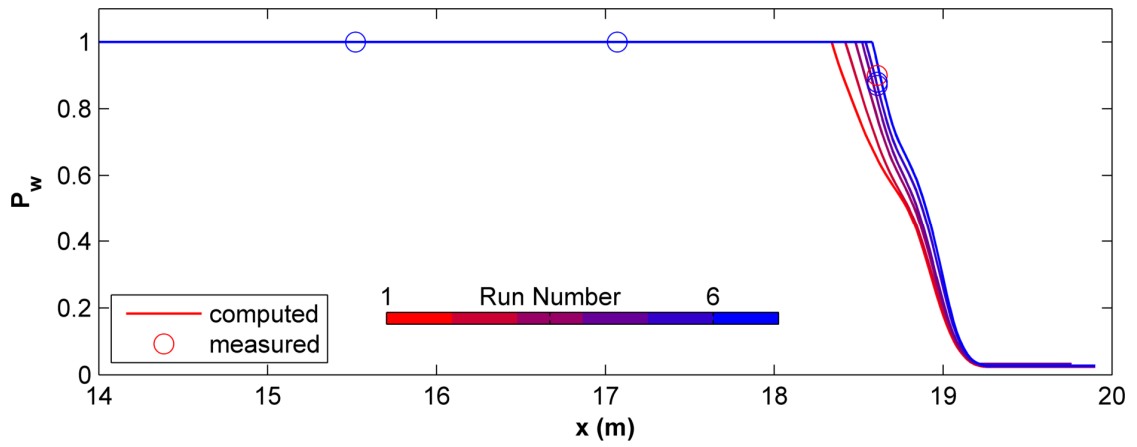


Figure B.12: Measured and computed wet probability  $P_w$  for the 6 runs of the SW test.

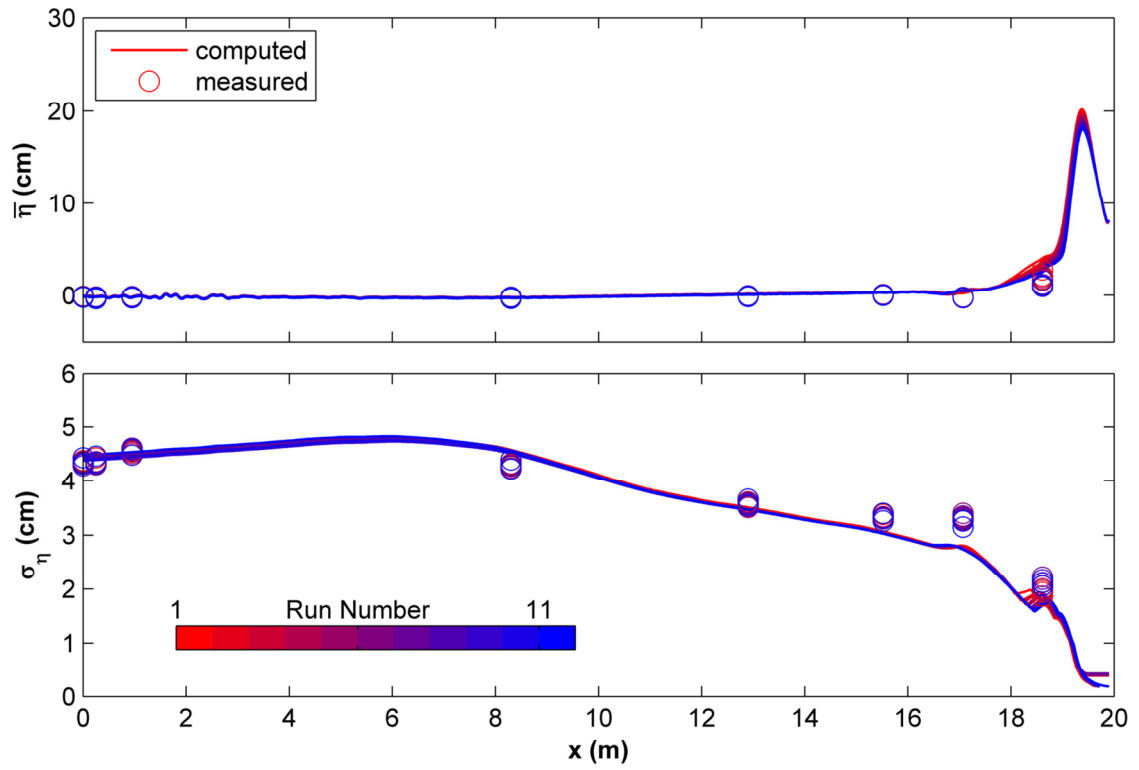


Figure B.13: Measured and computed mean (top) and standard deviation (bottom) of the free surface elevation  $\eta$  for the 11 runs of the TD test.

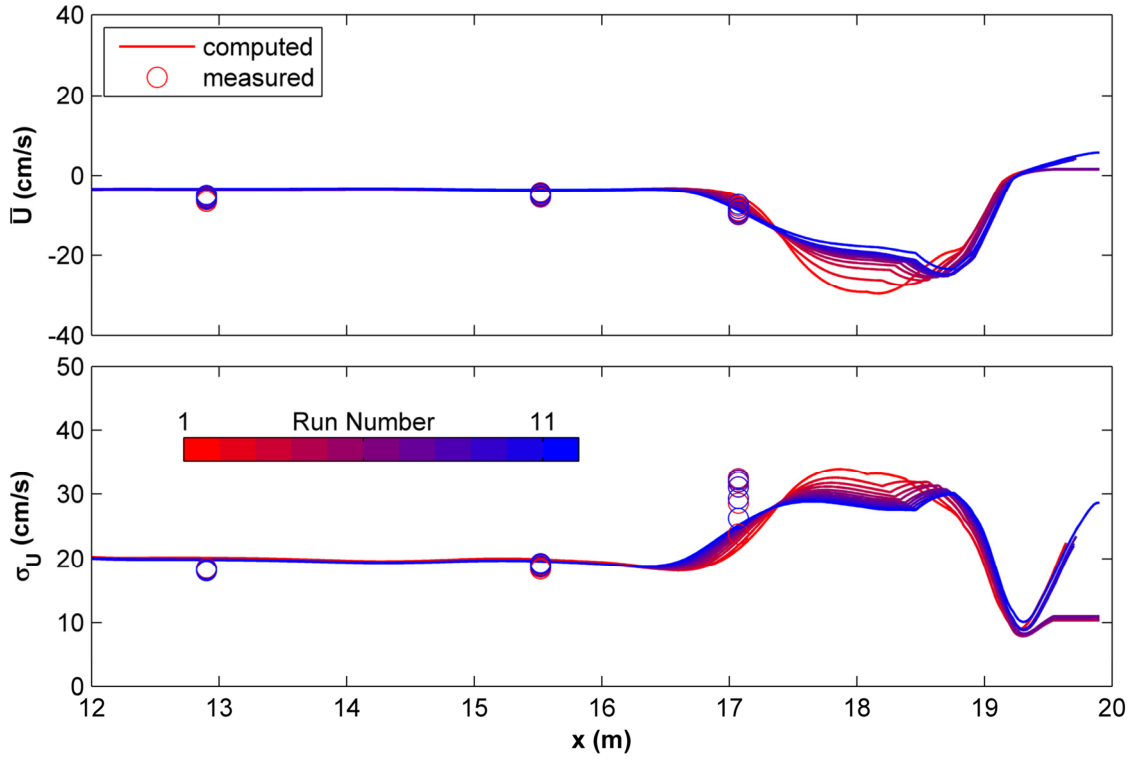


Figure B.14: Measured and computed mean (top) and standard deviation (bottom) of the cross-shore velocity  $U$  for the 11 runs of the TD test.

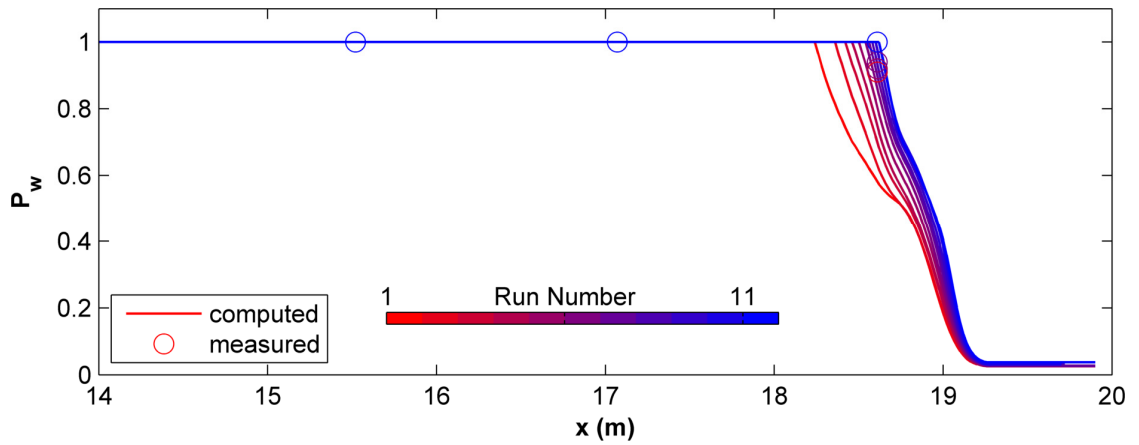


Figure B.15: Measured and computed wet probability  $P_w$  for the 11 runs of the TD test.

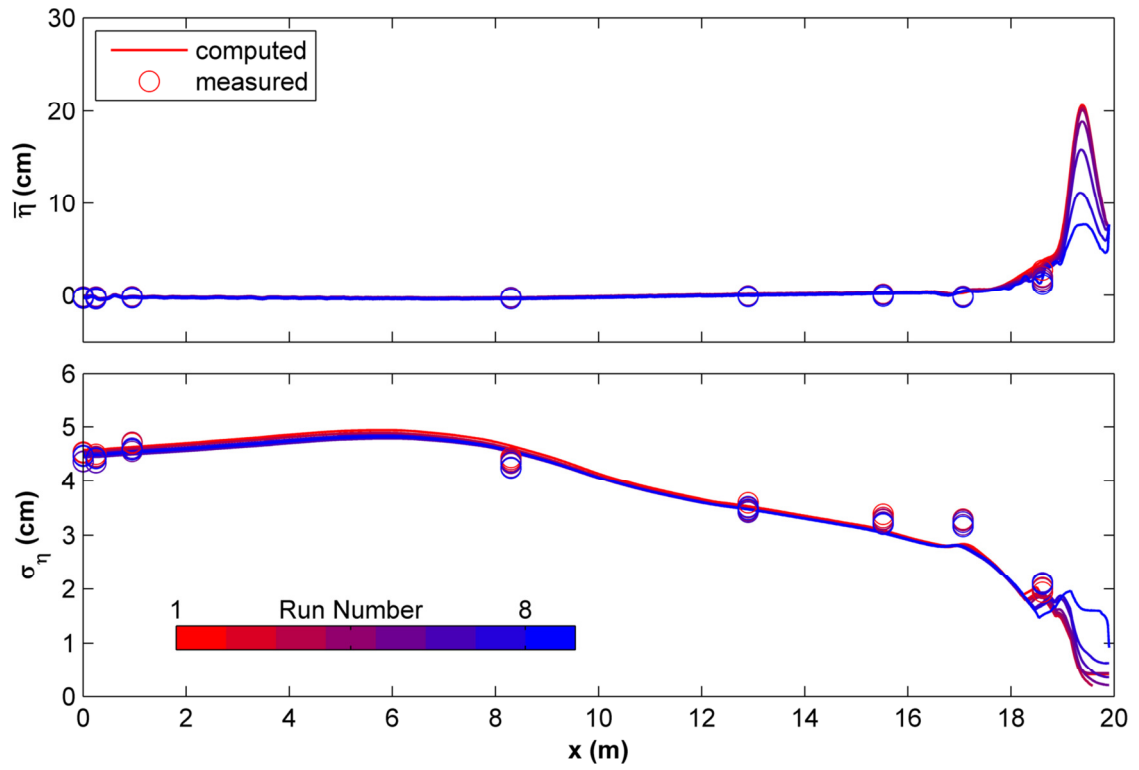


Figure B.16: Measured and computed mean (top) and standard deviation (bottom) of the free surface elevation  $\eta$  for the 8 runs of the TB test.

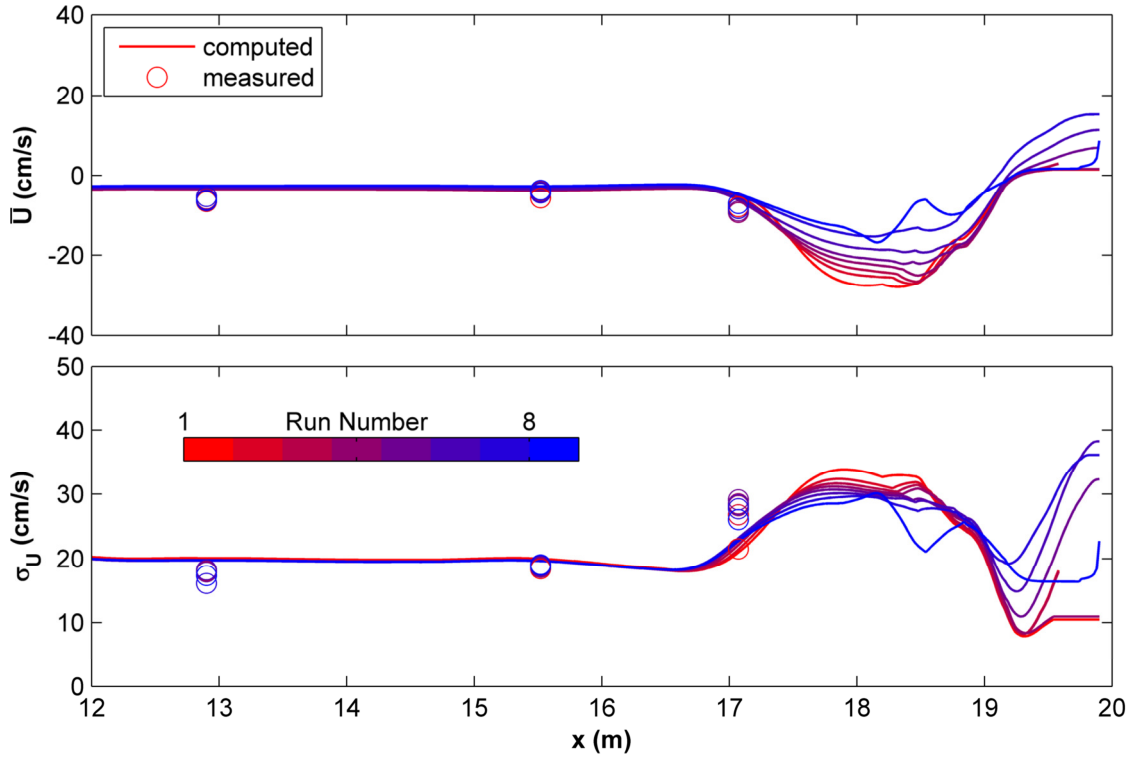


Figure B.17: Measured and computed mean (top) and standard deviation (bottom) of the cross-shore velocity  $U$  for the 8 runs of the TB test.

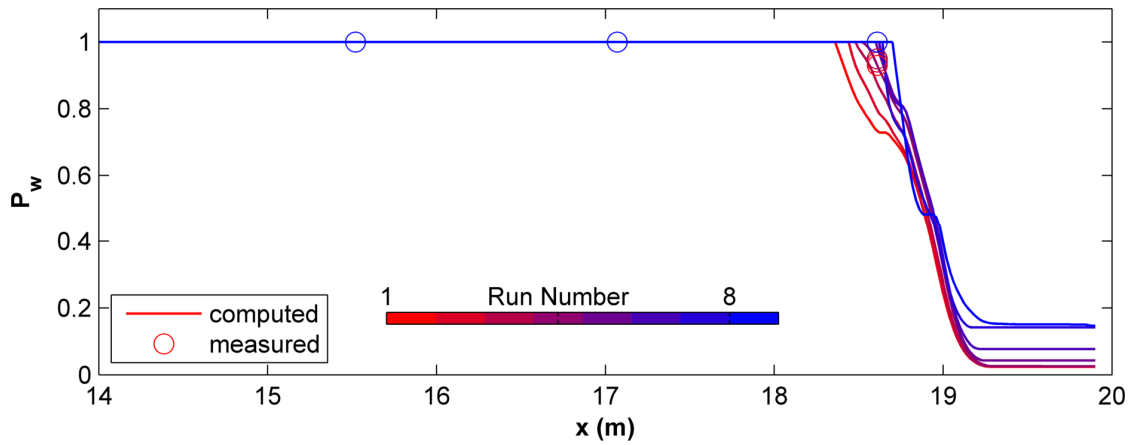


Figure B.18: Measured and computed wet probability  $P_w$  for the 8 runs of the TB test.

## Appendix C

### EXTREME FREE SURFACE AND VELOCITY COMPARISONS

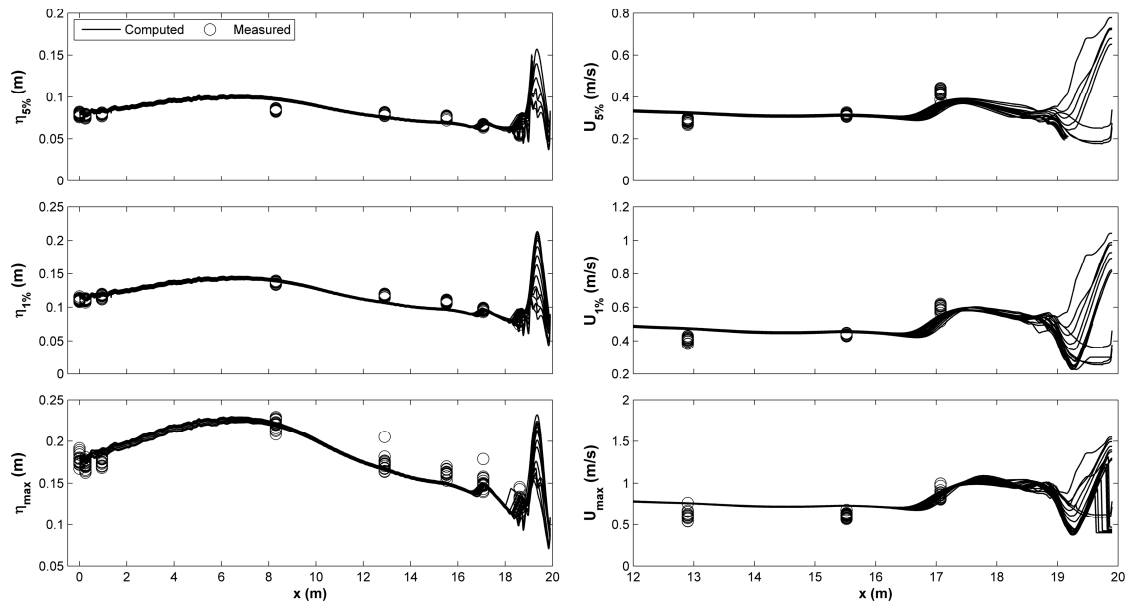


Figure C.1: Measured and computed cross-shore variations of free surface elevation  $\eta_e$  and onshore velocity  $U_e$  with exceedance probability  $e = 5\%$ ,  $1\%$ , and  $0.013\%$  for DN test.

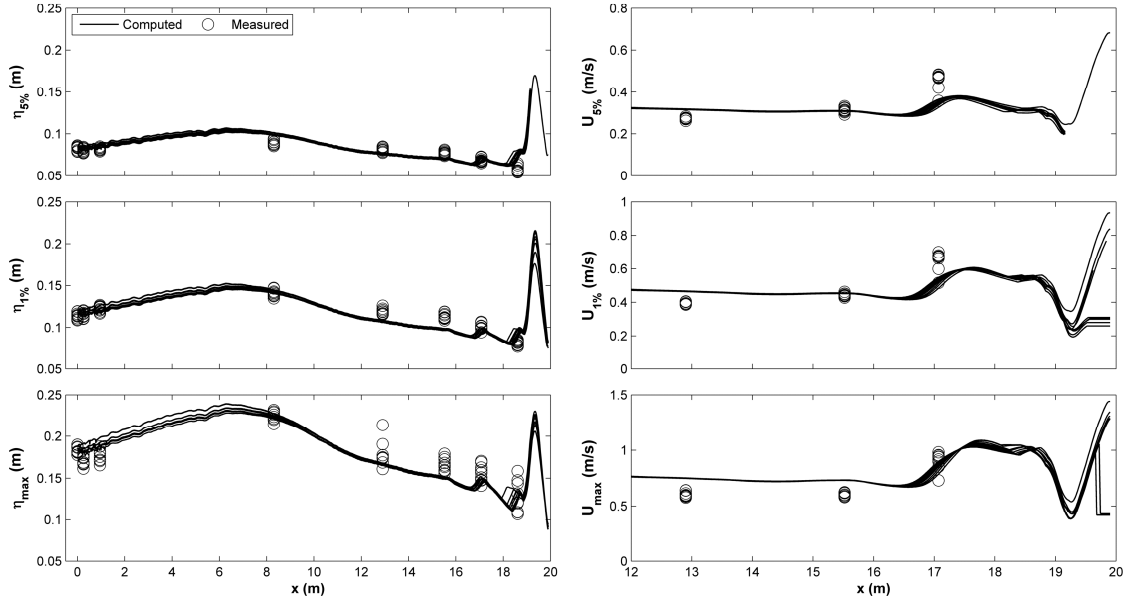


Figure C.2: Measured and computed cross-shore variations of free surface elevation  $\eta_e$  and onshore velocity  $U_e$  with exceedance probability  $e = 5\%$ ,  $1\%$ , and  $0.013\%$  for SN test.

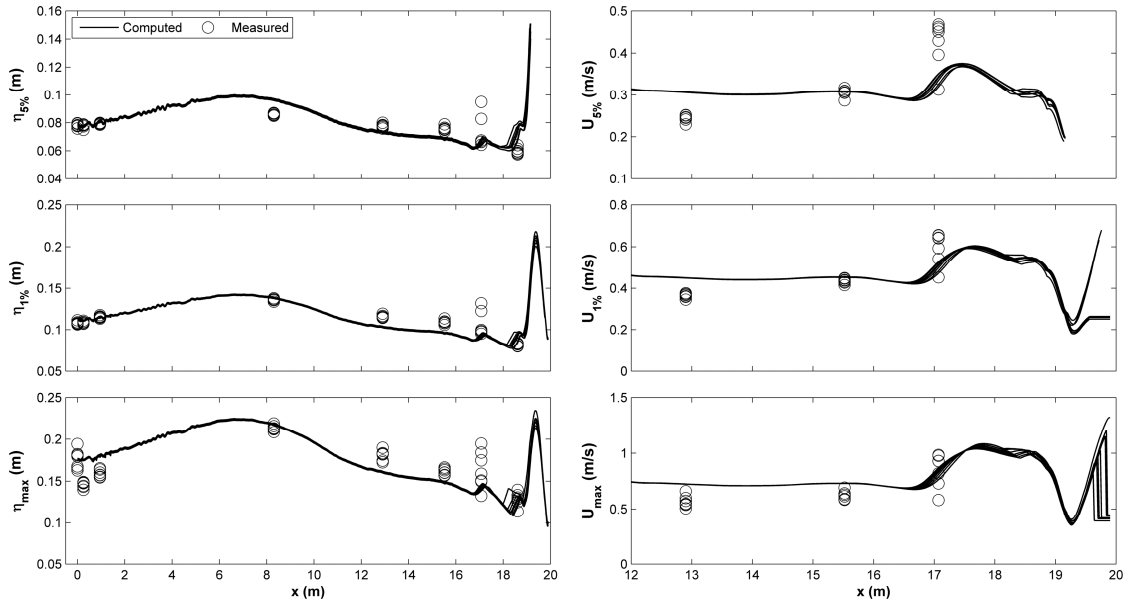


Figure C.3: Measured and computed cross-shore variations of free surface elevation  $\eta_e$  and onshore velocity  $U_e$  with exceedance probability  $e = 5\%$ ,  $1\%$ , and  $0.013\%$  for DW test.

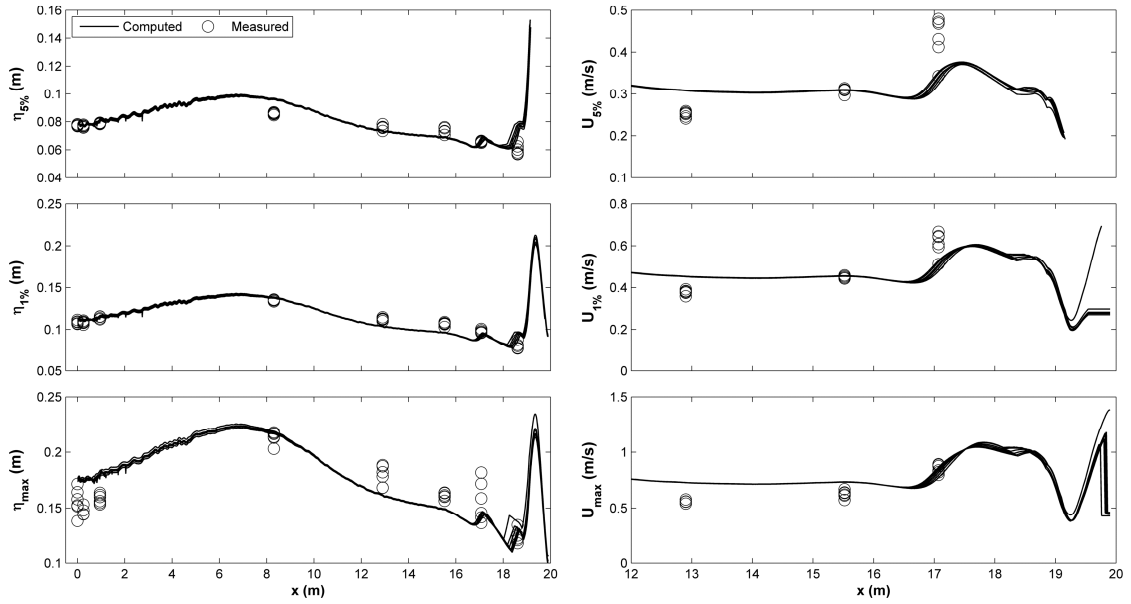


Figure C.4: Measured and computed cross-shore variations of free surface elevation  $\eta_e$  and onshore velocity  $U_e$  with exceedance probability  $e = 5\%$ ,  $1\%$ , and  $0.013\%$  for SW test.

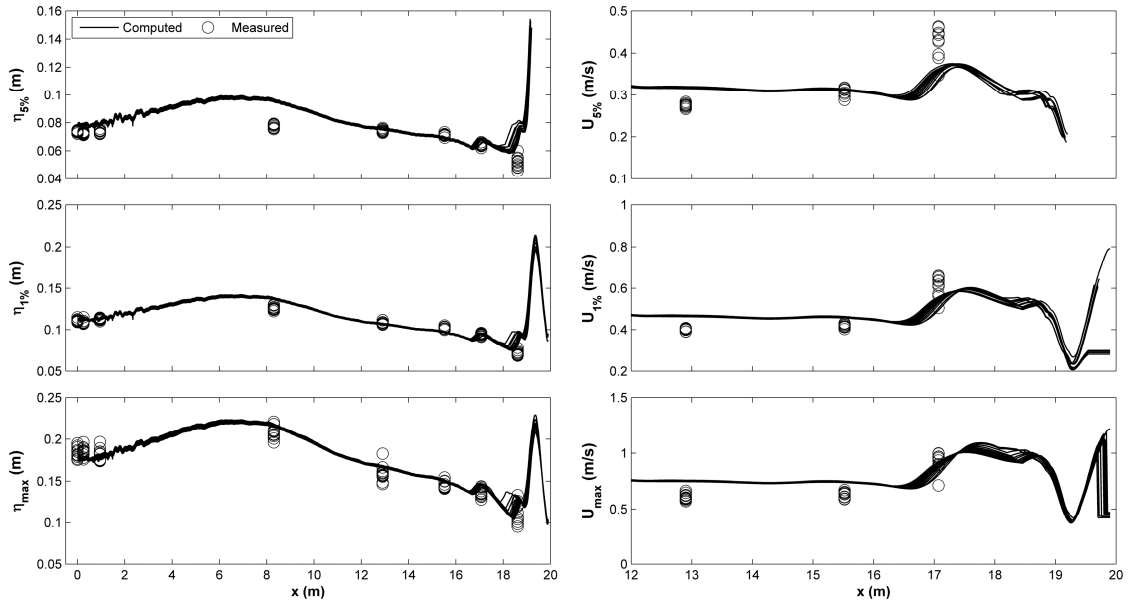


Figure C.5: Measured and computed cross-shore variations of free surface elevation  $\eta_e$  and onshore velocity  $U_e$  with exceedance probability  $e = 5\%$ ,  $1\%$ , and  $0.013\%$  for TD test.

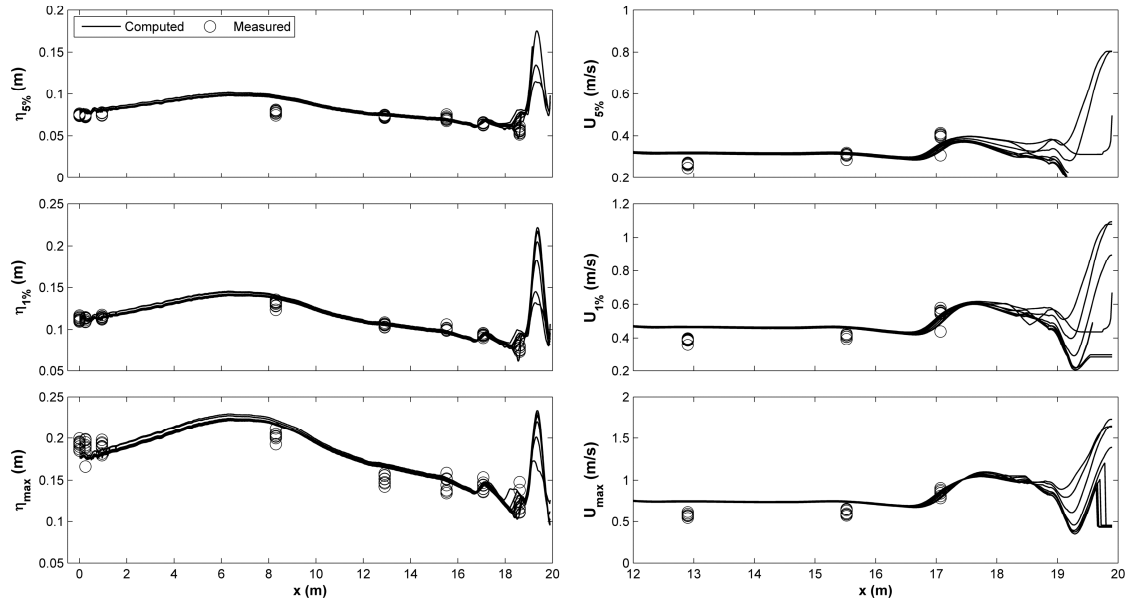


Figure C.6: Measured and computed cross-shore variations of free surface elevation  $\eta_e$  and onshore velocity  $U_e$  with exceedance probability  $e = 5\%$ ,  $1\%$ , and  $0.013\%$  for TB test.